iScience

CellPress
OPEN ACCESS

Article

Tunneling Nanotubes Mediate Adaptation of Glioblastoma Cells to Temozolomide and Ionizing Radiation Treatment

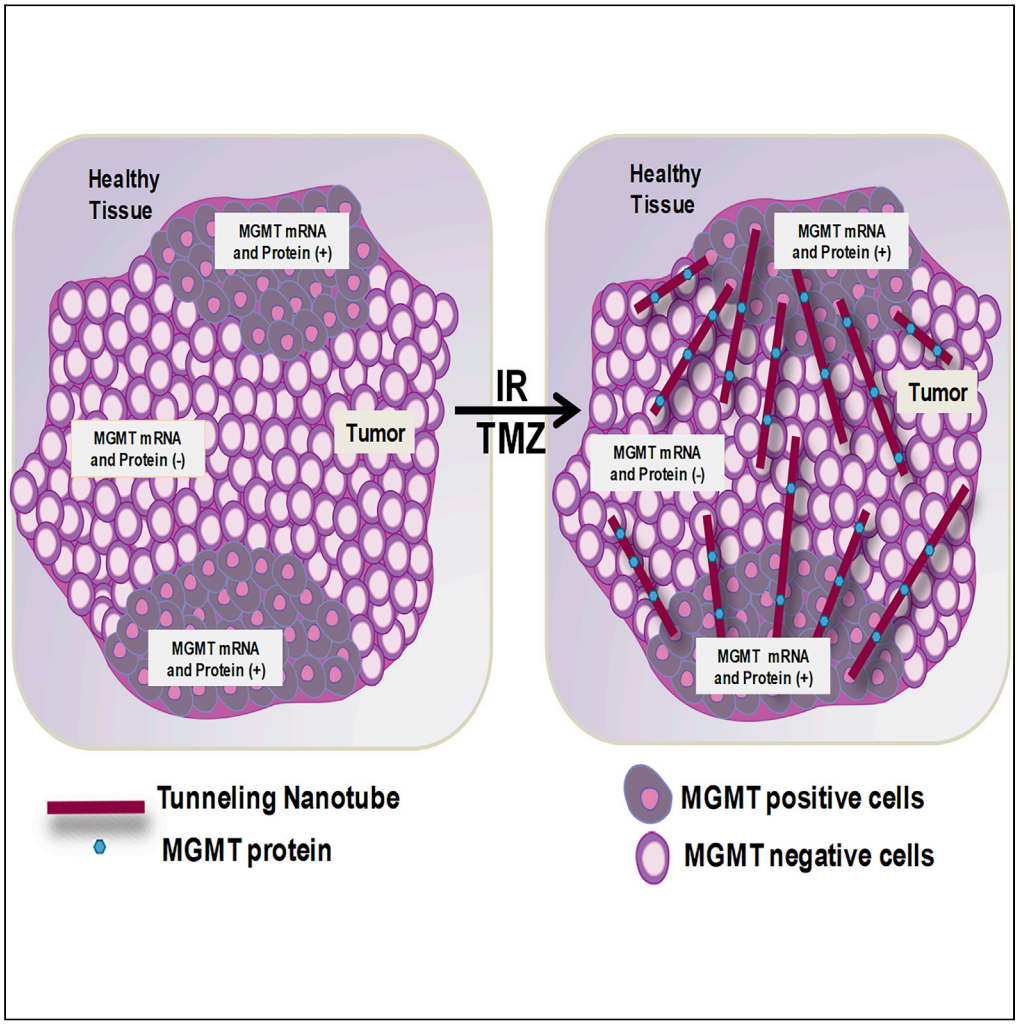

Silvana Valdebenito, Alessandra Audia, Krishna P.L. Bhat, George Okafo, Eliseo A. Eugenin

eleugeni@utmb.edu

HIGHLIGHTS

GBM cells form TNTs in response to ionizing radiation and TMZ treatment

TNTs transfer MGMT protein from resistant to sensitive cells to treatment

MGMT protein transferred via TNTs protect target cells from TMZ and IR treatment

Blocking TNTs and MGMT spread could prevent tumor adaptation to TMZ treatment

Valdebenito et al., iScience *23*, 101450
September 25, 2020
https://doi.org/10.1016/j.isci.2020.101450

iScience

CellPress
OPEN ACCESS

Article

Tunneling Nanotubes Mediate Adaptation of Glioblastoma Cells to Temozolomide and Ionizing Radiation Treatment

Silvana Valdebenito,[1] Alessandra Audia,[2] Krishna P.L. Bhat,[2] George Okafo,[3] and Eliseo A. Eugenin[1,4,*]

SUMMARY

Glioblastoma (GBM) is the most prevalent and aggressive tumor in the central nervous system. Surgical resection followed by concurrent radiotherapy (ionizing radiation [IR]) and temozolomide (TMZ) is the standard of care for GBM. However, a large subset of patients offer resistance or become adapted to TMZ due mainly to the DNA repair enzyme O^6-methylguanine-DNA methyltransferase (MGMT). Thus, alternative mechanisms of MGMT deregulation have been proposed but are heretofore unproven. We show that heterogeneous GBM cells express tunneling nanotubes (TNTs) upon oxidative stress and TMZ/IR treatment. We identified that MGMT protein diffused from resistant to sensitive cells upon exposure to TMZ/IR, resulting in protection against cytotoxic therapy in a TNT-dependent manner. *In vivo* analysis of resected GBM tumors support our hypothesis that the MGMT protein, but not its mRNA, was associated with TNT biomarkers. We propose that targeting TNT formation could be an innovative strategy to overcome treatment resistance in GBM.

INTRODUCTION

Glioblastoma (GBM) is a malignant brain tumor that remains a major treatment challenge in oncology. Historically, these tumors have been treated with maximal surgical resection, followed by external beam radiation therapy. Survival was extended by adding the alkylator temozolomide (TMZ) (Arora and Somasundaram, 2019; Jackson et al., 2019; Nam and de Groot, 2017; Thomas et al., 2017; Zhang et al., 2012b). Surgery followed by concurrent chemo-radiation remain the standard of care for patients with GBM. Despite the aggressive combined modality approach, the 2-year survival for patients with GBM remains only 10%–25%, and few patients survive beyond 5 years (Batash et al., 2017; Delgado-Lopez and Corrales-Garcia, 2016). Thus, new treatments are urgently needed.

TMZ tumor resistance has been associated with the expression and function of the DNA repair enzyme O^6-methylguanine-DNA methyl-transferase (MGMT). TMZ generates a methylation at the O^6 atom of guanine, O^6-methylguanine lesions, resulting in DNA mismatch, and subsequent apoptosis (Pegg, 2000; Silber et al., 2012). MGMT removes O^6-methylguanine DNA lesions preventing apoptosis of the tumor cells (Hegi et al., 2005; Pegg, 2000). Thus, tumor cells lacking MGMT are significantly more sensitive to the cytotoxic effects of TMZ than tumor cells expressing a functional MGMT protein (Hegi et al., 2005; St-Coeur et al., 2016). Currently, the most widely accepted mechanism of resistance to TMZ treatment has been associated with changes in MGMT expression due to promoter methylation (Hegi et al., 2005, 2019; Hegi and Stupp, 2015; Mansouri et al., 2019; Weller et al., 2010). Overall, it is believed that tumor cells expressing MGMT are resistant to TMZ treatment (Bahadur et al., 2019; Rahman et al., 2019; Zhang et al., 2012a). However, there is a lack of correlation between promoter methylation, MGMT enzymatic activity, tumor recurrence, and survival. Most of these inconsistencies have been associated with tumor heterogeneity, GB stem cells, cellular dedifferentiation, incomplete resection, or adaptation to treatment by unknown mechanisms (Arevalo et al., 2017; Zhang et al., 2012a). Also, analysis of MGMT promoter methylation indicates that only half of GBM expressed MGMT protein, suggesting alternative mechanisms of MGMT-mediated protection (Hegi et al., 2019; Mansouri et al., 2019; Preusser et al., 2008). Furthermore, several studies reported novel mechanisms for MGMT regulation such as the K-M enhancer activation (Abe et al., 2018; Chen et al., 2018b; Kim et al., 2019; Raghavan et al., 2020; Tsai et al., 2019; Wick and Platten, 2018; Yi et al., 2019), highlighting

[1]Department of Neuroscience, Cell Biology, and Anatomy, University of Texas Medical Branch (UTMB), Research Building 17, Fifth Floor, 105 11th Street, Galveston, TX 77555, USA

[2]Department of Translational Molecular Pathology, Division of Pathology and Laboratory Medicine, M.D. Anderson, Houston, TX, USA

[3]GO Pharma-consulting Ltd., Welwyn, UK

[4]Lead Contact

*Correspondence: eleugeni@utmb.edu

https://doi.org/10.1016/j.isci.2020.101450

the complexity of TMZ resistance and the need to consider additional mechanisms of MGMT-mediated tumor protection and adaptation to treatment.

Tunneling nanotubes (TNTs) are cellular processes that enable cell-to-cell communication at long range, from 30 to 500 μm distance. Normally, TNTs participate in key biological processes, including development, signaling, and immune response (Ariazi et al., 2017a; Okafo et al., 2017; Roehlecke and Schmidt, 2020), but TNT expression during adulthood is minimal. However, upon the development of several diseases, including viral and bacterial infection, cancer, synucleinopathies (Parkinson disease, Lewy bodies, and multiple system atrophy) and tauopathies, and prion-associated diseases, TNTs proliferate. TNT communication is used as highways to transfer and exchange viral/bacterial and cellular products as well as organelles, small molecules, vesicles, and second messengers from one cell to another (Abounit et al., 2015, 2016b; Gerdes et al., 2013). However, its role in disease is still under active investigation, and cancer is one of the key areas that need to be addressed in an urgent manner as described by multiple groups working in the area (Abounit et al., 2016a, 2016b; Abounit and Zurzolo, 2012; Austefjord et al., 2014; Desir et al., 2016; Eugenin et al., 2009b; Gerdes and Carvalho, 2008; Gerdes et al., 2013; Gousset et al., 2009; Souriant et al., 2019; Tardivel et al., 2016; Wang and Gerdes, 2012).

Here we demonstrate that GBM cells contain an active network of TNT-mediated communication under stress conditions, including oxidative stress and cytotoxic treatments. TNT formation and associated transport enable the transmission of the MGMT protein from MGMT mRNA-positive cells, which are resistant to TMZ/ionizing radiation (IR) treatment, into cells with low MGMT protein, which are susceptible to TMZ/IR TMZ treatment. The transfer of the MGMT protein by TNTs results in the protection of the target sensitive cells to TMZ/IR treatment. Our data demonstrate that TNT communication provides a novel mechanism of TMZ/IR resistance in GBM.

RESULTS

TNTs Are Induced by Oxidative Stress in GBM Cells

Many groups, including our own, have demonstrated that TNTs are induced in several cell types under infectious and cancer conditions (Ady et al., 2016; Ariazi et al., 2017b; Eugenin et al., 2009a; Okafo et al., 2017; Valdebenito et al., 2018). In contrast, a low number of TNTs are expressed during healthy conditions. Overall, TNTs are induced during pathological states (Okafo et al., 2017).

We used time-lapse microscopy to identify and quantify TNT stability, length, associated vesicular transport, collapse, and branching (still pictures every 0.5 or 1 min for 24–48 h). The metric for TNT identification was based on a strict criterion as seen in several key publications on TNT, including ours (Austefjord et al., 2014; Eugenin et al., 2009b; Gerdes et al., 2007; Osswald et al., 2015; Weil et al., 2017), as well as our preliminary data as follows. First, TNTs are distinct from filopodia: *in vitro* TNTs are located on the top optical plane of the cell, whereas filopodia are in the bottom optical plane. Thus, TNTs are generated from a different cellular structure than filopodia. Currently, in primary cells (neurons, astrocytes, macrophages, T cells, and microglia) or our cell lines, we do not have any evidence that filopodia become TNTs; both are distinct structures. Second, TNTs do not attach to a substrate as filopodia; instead, they are free-standing. Third, TNTs communicate two or more cells at a minimal distance of 30 μm. Fourth, the TNT process can branch and reach distances up to 500 μm. Fifth, TNTs can transport organelles, vesicular structures, and small molecules between TNT connected cells. Sixth, TNTs are positive for actin and negative or poorly positive for tubulin, a key difference with filopodia, which are positive for both (Ariazi et al., 2017b; Astanina et al., 2015; Polak et al., 2015). Last, TNTs are positive for several TNT markers not present in filopodia, including Tweety-homolog 1 (TTHY1), GAP43, and protein 14-3-3γ, as described in Jung et al. (2017).

To perform our experiments, two well-characterized GBM cell lines (U87 and T98G) were selected based on TMZ/IR treatment sensitivity, cell size, and genetic signature. First, pure cultures of U87 and T98G cells were subjected to oxidative stress (H_2O_2, 100 μM) and TMZ/IR treatment and live-cell imaging were performed to analyze TNT formation, stability, length, vesicular transport, and branching. We observed that both GBM cell lines under untreated conditions exhibit minimal TNT formation at baseline (Figure 1). Quantification of TNT was performed using an imaging software, NIS elements, using the criteria described earlier.

Previous studies have shown that oxidative stress induced by H_2O_2 treatment of human mesenchymal stem cells induces the formation of TNTs (Wang et al., 2011; Zhang and Zhang, 2015; Zhu et al., 2005). Treatment

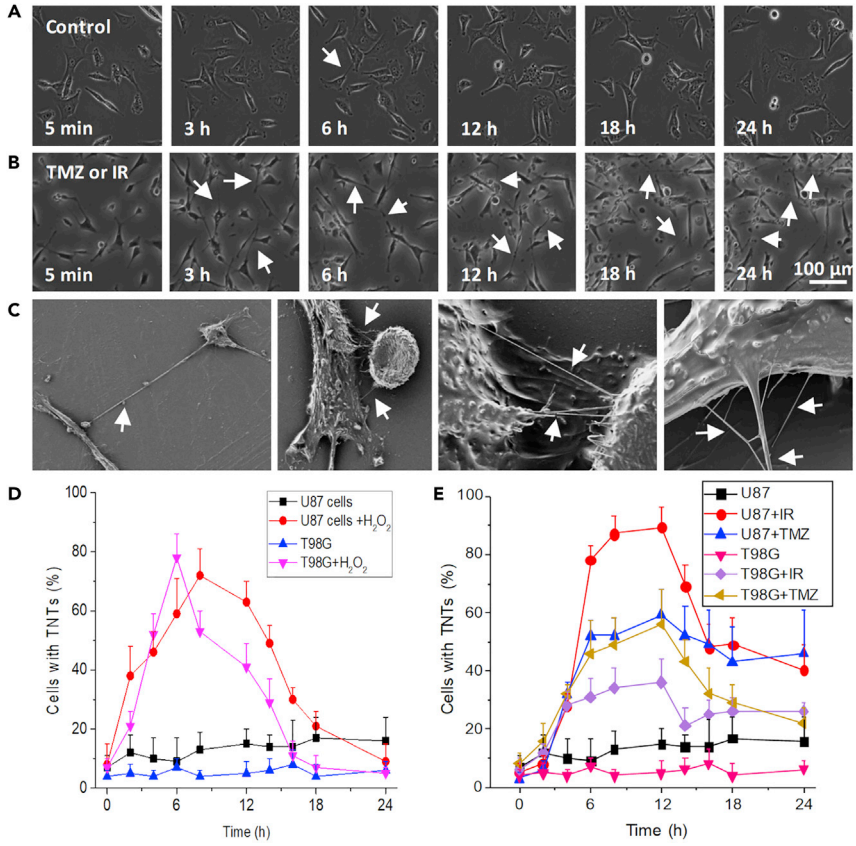

Figure 1. TNTs Are Induced in GBM Cells in Response to Oxidative Stress, Radiation (IR), and TMZ Treatment

(A) Live-cell imaging for U87 and T98G for 24–48 h with still pictures every 30 s to 1 min to identify, quantify, and characterize TNT formation, stability, collapse, and associated transport. Representative still pictures after 5 min and 3, 6, 12, 18, and 24 h. In the control condition, minimal numbers of cells with TNTs were detected (arrows represent TNTs).

(B) Upon treatment with H_2O_2 (100 μM), IR (3, 6, 9, or 12 Gy, only 6 Gy is shown in (B), or TMZ (50 μM) TNTs proliferate (arrows represent TNTs).

(C) Representative scanning electron microscopy of cultures of GBM cells subjected to TMZ/IR treatment. Arrows denote TNTs.

(D) Quantification of cells with TNTs in pure cultures of U87 or T98G in the presence and absence of H_2O_2 treatment.

(E) Quantification of TNT formation in U87 or T98G cells subjected to IR treatment (6 Gy) and TMZ as a function of time. All curves and points after 3 h were significant when compared with untreated controls ($p \leq 0.024$, n = 6–9, data are expressed as mean ± SD).

of U87 or T98G cells with H_2O_2 (100 μM) induces the formation of TNTs in a time-dependent manner (Figure 1D). In addition to the increased numbers of cells with TNTs (Figure 1D), we also detected an increased TNT stability (transient, less than 5 min, or stable TNT, more than 5 min, depending on the duration of the TNT contact), length (short, up to 30 μm, and long TNTs, longer than 30 μm), associated vesicular transport, and TNT branching in response to oxidative stress (see a summary of the data in Table S1). Electron microscopic analysis confirmed our live-cell imaging data that TNTs proliferate in response to oxidative stress (Figure 1C). Under electron microscopy each TNT observed or quantified by live-cell or confocal imaging was constituted of several tangled smaller TNTs, and each TNT can branch from several areas of the plasma membrane to contribute to TNT formation. Thus, several potential permeabilities, based on size and diameter, may be present in GBM cells in a similar manner to that in HIV-infected macrophages, as we described (Okafo et al., 2017).

Examination of additional inflammatory conditions that induced TNTs in immune cells failed to induce the formation of TNTs in GBM cell lines including tumor necrosis factor-α or lipopolysaccharide plus interferon-γ (100 ng/mL) or HIV-gp120 (50 ng/mL) (data not shown) as we previously described (Eugenin et al., 2001, 2003), suggesting that general cell activation is not a condition that induces TNT formation in GBM cells. In

addition, media from one cell into another do not induce TNT formation. Thus, TNT formation is stress-induced, but the directed TNT communication between different populations of cells is controlled by an unknown mechanism.

TNTs Are Induced by TMZ/IR Treatment in GBM Cells

To examine whether differences in sensitivity to TMZ/IR treatment can distinguish TNT formation, we compared two well-established GBM cell lines, U87 and T98G. Both cell lines have significant differences in sensitivity to TMZ/IR treatment. Pure cultures of U87 cells are sensitive to TMZ (IC_{50}: 10 μM) and IR treatment (Lee, 2016; Towner et al., 2019). In contrast, pure cultures of T98G cells are resistant to TMZ (IC_{50}: 500 μM) and IR treatment (Lee, 2016; Melamed et al., 2018; Towner et al., 2019) (see summary in Table S2). Also, under unstimulated conditions, both cell types have low levels of TNT communication (5%–10% of cells had TNTs, Figures 1D, 1E, and S1). Surprisingly, in a similar manner to oxidative stress, IR (3 and 12 Gy, Figures 1B and 1E) and TMZ (Figure 1E and Table S1) treatment increased the formation of TNT in a time-dependent manner (Figure 1E). The increase in TNT numbers induced by TMZ and/or IR treatment was associated with enhanced TNT stability (transient or stable TNT, depending on the duration of the TNT contact), length (short and long), associated vesicular transport, and branching of the TNT process (see a summary of the data in Table S1). Our data demonstrate that chemo-radiation treatment of GBM cells promotes TNT formation.

TNTs Are Induced by Stress or TMZ/IR Treatment

Only recently has it been demonstrated *in vivo* that Tweety-Homolog 1 (TTHY1), GAP43, and 14-3-3γ proteins are present in TNTs, and they are potent drivers of tumor colonization and growth (Jung et al., 2017). Thus, to examine whether TNTs participate in tumor resistance to TMZ/IR treatment, we developed a co-culture system between GBM cells that are resistant and sensitive to TMZ/IR treatment, as described in Table S2. The co-culture model contains resistant T98G cells at the center of the plate, whereas treatment-sensitive cells (U87) were at the periphery of the plate. Both cell types are initially separated by a silicon ring of a width of 50–150 μm (see model, Figures 2A and 2B to see the interface between both cell types); however, upon removal of the silicon ring, both cell types establish TNTs allowing the quantification of TNTs in T98G (resistant cells to TMZ/IR), the interface between both cell types, and U87 cells (sensitive cells to TMZ/IR treatment) can be observed and quantified by live-cell imaging (Figure 2B and see Transparent Methods). Figure 2C corresponds to a representative image of TNTs between resistant and sensitive cells at the interface area stained for DAPI (blue staining, nuclear), protein 14-3-3-γ (Figure 2C, red staining, TNT marker), and actin (phalloidin, white staining) (Figure 2C). Control experiments using labeled cells with DiI or mitotracker staining or taking the medium from one cell type and adding to the other did not contribute to the data shown below. Thus, overall, our data indicate that most processes detected are TNTs and not filopodia according to our definition of TNTs. Our central hypothesis for the enhanced TNT formation induced by H_2O_2, TMZ, and/or IR corresponds to a rescue and adaptation mechanism of the tumor to prevent the apoptosis of cancer cells.

As described in Figure 1, live-cell imaging was performed to evaluate the time course of TNT formation using our co-culture tissue culture model. Oxidative stress and TMZ/IR induce TNT formation (Figure S1). These stress conditions also resulted in increased TNT stability, length, associated vesicular transport, and TNT branching, as described in Figure 1 and Table S1. Furthermore, as shown in Figure 2D, untreated cultures of resistant or sensitive GBM cells had a minimal formation of TNTs (5%–10% of the total population) even when cultured in separate chambers (Figure 2D). Quantification of TNTs in untreated co-culture indicated a minimal number of cells expressing TNTs even when the silicon ring was removed (Figure 2D).

Using the co-culture between U87 and T98G cells, oxidative stress and H_2O_2 increased TNT numbers in both cell types, but more important increased TNT further between both cell types (Figure 2E, T98G, U87, and interface). A similar pattern of homo- and hetero-TNT communication was observed for TMZ treatment (50 μM). Interestingly, the homo-cellular communication induced by oxidative stress or TMZ/IR treatment observed in the co-culture did not reach the TNT levels observed in pure cultures after 3, 6, 12, 24, and 48 h, the last point assayed (~80%, compared with Figure 1).

In contrast, TNT formation in response to TMZ treatment at the interface between both cell types increased to a near 100% of the cells having TNTs (Figure 2F, *$p \leq 0.005$ when compared with untreated cells, #$p \leq 0.001$ when compared with T98G or U87 cells). Similar results of TNT formation were found after IR

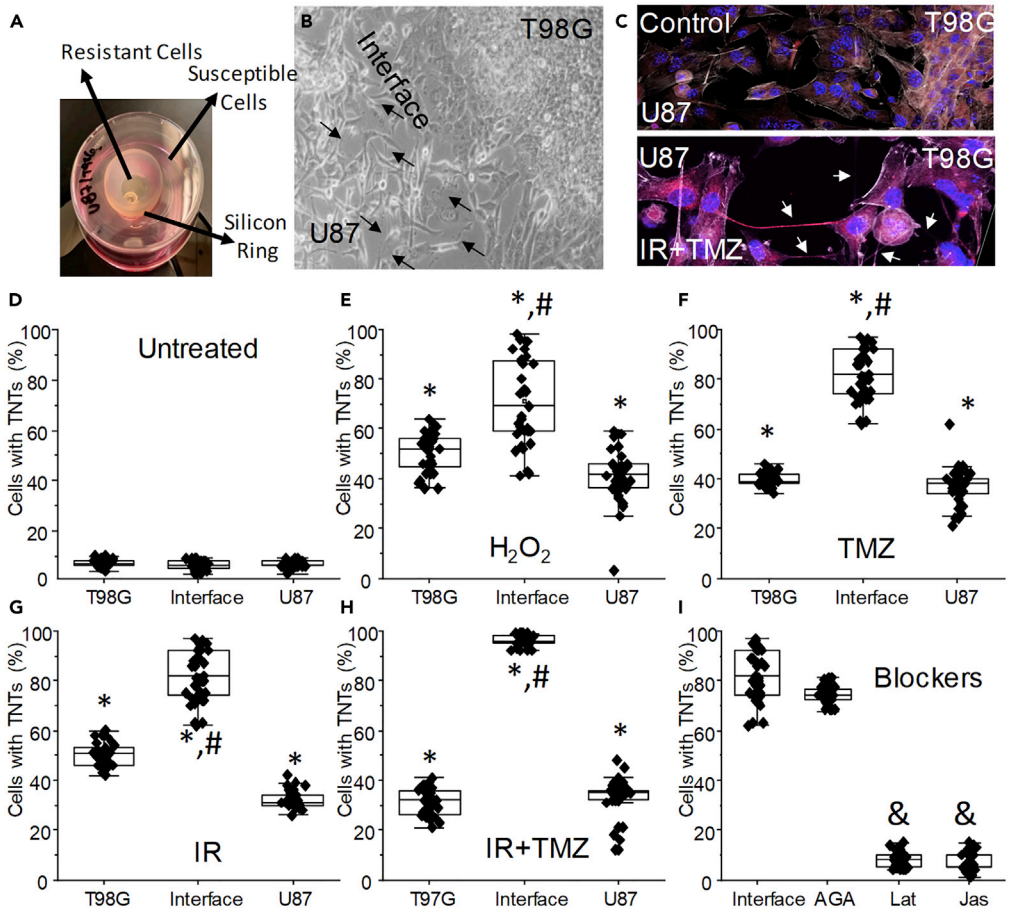

Figure 2. TNT Formation between Different GBM Cells Is Regulated by Oxidative Stress and TMZ/IR Treatment

(A) To examine the role of TNTs in response to TMZ and IR treatment, we generate a co-culture system between GBM cells resistant (T98G) and sensitive (U87) to TMZ/IR treatment (see Table S2 for details). The co-culture system consists of both cell types separated by a silicon ring. Removal of the silicon ring in a specific location enables the quantification of TNTs in different areas of the plate.

(B) At the interface of both cell types, TNT could be easily identified and quantified by live-cell imaging. Arrows denote TNTs formed between both cell types.

(C) Confocal microscopy at the interface between both cell types under control and TMZ/IR treatment (TMZ + IR). Arrows denote TNTs between both GBM cell types.

(D) Quantification of TNTs in our co-culture system under control conditions. The co-culture is composed of T98G, interface, and U87 cells.

(E) Quantification of TNTs after 12–24 h post H_2O_2 treatment in our co-culture system.

(F) Quantification of TNTs after 12–24 h post-TMZ treatment in our co-culture system.

(G) Quantification of TNTs after 12–24 h post IR treatment (6 Gy) in our co-culture system.

(H) Quantification of TNTs after 12–24 h post-TMZ/IR treatment in our co-culture system.

(I) Quantification of TNTs only at the interface between both cell types in the presence of the gap junction blocker, 18-alpha-glycyrrhetinic acid (35 μM, AGA). We previously demonstrated that blocking gap junctions did not prevent TNT formation but reduced associated transport. TNT blockers, latrunculin or jasplakinolide (10 nM), prevented the formation of TNTs at the interface. *$p \leq 0.005$ when compared with untreated cells; #$p \leq 0.005$ when compared with T98G cells in the same co-culture; &$p \leq 0.005$ when compared with TMZ/IR at the interface between both cell types, n = 5–7, data are expressed as mean ± SD.

treatment (3, 6, and 12 Gy, Figure 2G). The combination of TMZ/IR treatment also increased TNT formation (Figure 2H). Surprisingly, when both cell types were cultured after TMZ/IR treatment, most TNTs were formed from T98G to U87 cells (85.87% ± 10.6%, n = 19, corresponds to TNTs at the interface from T98G into U87 cells, suggesting a directed communication). No TNTs from U87 to T98G were detected, suggesting that upon treatment (TMZ and/or IR), T98G cells detect U87 cells to establish TNT

communication, and U87 cells are only a recipient of the TNT process mostly formed from T98G cells. However, the mechanism of formation and identification of cells lacking TMZ/IR protection is unknown.

As we recently described in human primary macrophages, gap junctions at the tip of the TNTs are essential for cell-to-cell communication but not for TNT formation (Okafo et al., 2017). In agreement, 18α-glycyrrhetinic acid (35 μM) treatment did not alter the formation of TNTs when compared with TMZ/IR treatment (Figure 2I, interface). In contrast, latrunculin (Lat) or jasplakinolide (Jas), mild F-actin blocking agents, prevented the formation of TNTs (Figure 2I). Both Lat and Jas were used at a low concentration (10 nM), which would not affect the trafficking of several membrane receptors, including CCR5, CXCR4, and LRP1, mitochondria, or vesicular movement (see Figure S2). All these processes are highly dependent on actin trafficking (Ding et al., 2003; Kuang et al., 2012). Also, the quantification of filopodia during the time course analyzed did not change in the presence of these blockers (no significant change in the numbers of filopodia per cell or polarity even in the presence of TNT formation was found). In addition, soluble factors released for untreated or TMZ- and/or IR-treated T98G cells into U87 cultures did not induce TNTs (6.95% ± 5.43% of cells with TNTs). TNT formation was independent of the flow of the media because if the experiment was performed in a flow chamber to control the movement of soluble molecules between the two cell types no protection was communicated to the sensitive cells in response to TMZ and/or IR (data not shown). In conclusion, TNTs are induced between different GBM cells upon "stress" conditions in a unidirectional manner.

TNT Formation between Resistant and Sensitive Cells Enables Sensitive Cells to Become Resistant to TMZ/IR Treatment

Using our co-culture system described earlier in the article, we subject the GBM cell lines to TMZ/IR treatment in the presence and absence of TNT blockers (Lat, 10 nM, Figure 3, or Jas, data not shown) to determine their percentage of survival (Figures 3A–3F). To mimic the therapy currently used in patients with GBM, we included TMZ treatment (50 μM) in the analysis. TMZ concentration was selected as it corresponds to the serum concentration achieved in humans using a standard protocol of 150 mg/m^2 per day (Melamed et al., 2018). Consistent with previous reports, isolated cultures of U87 cells were sensitive to TMZ/IR and showed reduced survival (Figures 3B and 3C, red and blue line, respectively, U87-U87) when compared with T98G cells that were resistant to IR (Figures 3B and 3C, black line, T98G-T98G). Using the co-culture system described earlier, we determined whether TNT formation between both cell lines can transfer TMZ/IR protection from resistant cells, T98G, into sensitive cells, U87. As described in Figures 3B and 3C, T98G cells are resistant to TMZ/IR treatment (black lines, T98G-T98G). The addition of TMZ to T98G cells did not alter their survival in the presence of IR (Figure 3C, red line, T98G-T98G + TMZ). U87 cells were sensitive to TMZ/IR treatment (Figure 3C, blue and pink lines, U87-U87 and U87-U87 + 50 μM TMZ, respectively). Co-culture of T98G cells forming TNTs with U87 cells was protective against cell death induced by TMZ and IR treatment in U87 cells (Figure 3C, green and dark blue line, T98G-U87 and T98G-U87 + 50 μM TMZ, respectively, only U87 cells were quantified) indicating that T98G cells upon TNT formation transfer a TMZ/IR protective factor into U87 cells. Blocking the formation of TNT with Lat 2 h after treatment prevented the adaptation of U87 cells to TMZ/IR treatment (Figure 3C, purple line, T98G-U87 + Lat). In conclusion, our data demonstrated that TNT formation between different tumor cells could transmit chemo- and radio-resistance from GBM-resistant cells to GBM-sensitive cells preventing their apoptosis in response to TMZ/IR treatment.

To demonstrate that soluble factors did not mediate the TNT-mediated adaptation of sensitive cells to TMZ/IR treatment, media from untreated and TMZ/IR-treated T98G cells were collected at different time points (1, 3, 7, and 14 days) and applied to sensitive cells. Treatment of U87 cells with the medium collected from T98G without removing the barrier did not induce adaptation of U87 cells to TMZ/IR treatment (Figure 3D, T98G-barrier-U87 + TMZ + medium, pink line). Thus, the conditioned medium was not sufficient to provide the TMZ/IR protection of sensitive cells as described for TNTs.

Our data also demonstrated that at least 6–12 h of constant TNT formation between resistant cells, T98G, and sensitive cells, U87, to TMZ/IR treatment was required to observe the TNT-mediated transfer of the protective factor(s). The early addition of Lat or Jas after 2 h post-TNT contacts between both cell types prevented the adaptation of sensitive cells to become resistant to therapy, further confirming the requirement of TNT formation for the gain of resistance to TMZ/IR treatment (Figure 3E, T98G-U87 + lat or jas 2 h after TNTs, pink line). For TMZ + IR survival of sensitive cells, a TNT communication with resistant cells for at least 6 h was required to observe a significant amount of protection. Furthermore, to demonstrate that TNT

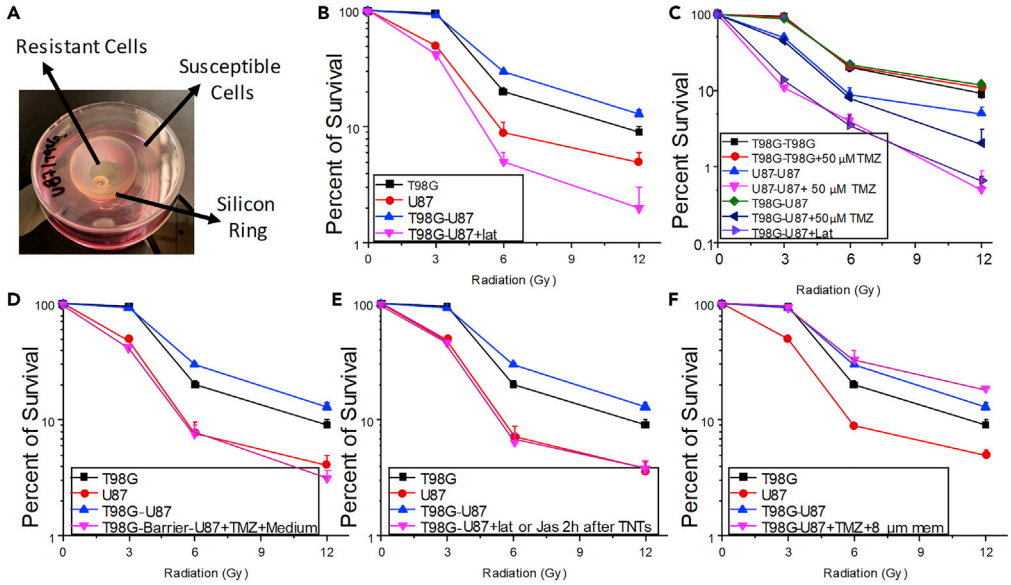

Figure 3. TNTs Enable the Communication between Heterogeneous GBM Cells Resulting in the Transfer of Protective Factors against TMZ/IR Treatment

To evaluate the role of TNTs in GBM, we determined the survival of GBM cultures alone or in co-culture in the presence and absence of TNTs after treatment with TMZ/IR.

(A) Our co-culture model to examine TNT formation as described in the previous figure. The co-culture system was used in the subsequent experiments, only quantifying the survival of U87 if both cell types are in the same co-culture.

(B) Evaluation of radiosensitivity of T98G (black line), U87 (red line), and our co-culture system (T98-U87, blue line). In the co-culture system, only the survival of U87 cells was quantified as T98G is resistant to treatment. The addition of latrunculin (lat, pink line) or jasplakinolide (data not shown) after 2 h post-treatment prevented the adaption of U87 provided by T98G cells and TNT formation to become resistant to TMZ/IR. For all points, after 3 Gy, only two groups were observed. U87 and T98G-U87 + lat were significantly different from T98G and T98G-U87 curves, n = 5, $p \leq 0.002$. Data were expressed as mean ± SD.

(C) TNTs formed between T98G and U87 cells induced the adaptation of U87 to become resistant to treatment. Blocking TNTs with lat prevented the adaptation of U87 cells to TMZ/IR treatment (T98G-U87 + lat). For all points after 3 Gy, three groups were observed. Group 1, U87-U87 + 50 μM TMZ and T98G-U87 + Lat; group 2, U87-U87 and T98G-U87 + 50 μM TMZ; group 3, T98G-T98G, T98G-U87, and T98G-T98G+50 μM TMZ, n = 6, $p \leq 0.001$ when compared with group 1. Data were expressed as mean ± SD.

(D) Medium from untreated and TMZ + IR-treated T98G cells cannot provide TMZ/IR protection to sensitive cells, U87. Using our co-culture system, we treated with TMZ and IR. Medium from T98G cells was collected at different time points and added to U87 cells. Overall, no transfer of protection against TMZ and IR was found in U87 cells (T98G-barrier-U87 + TMZ + medium). Thus, U87 cells still after treatment were susceptible to TMZ and IR treatment. For all points after 3 Gy, two groups were observed. Group 1, T98G and T98G-U87; and group 2, U87 and T98G-barrier-U87 + TMZ + Medium, n = 3, $p \leq 0.005$. Data were expressed as mean ± SD.

(E) To demonstrate that active TNT formation and the transport was required for the transfer of the protective factor against IR and TMZ treatment into U87 cells, we added TNT blockers after 2–6 h post-TNT formation (representative example after 2 h is shown, T98G-U87 + Lat or Jas after 2 h TNTs), which indicates that at least 6–12 h was required to transfer the protective factor(s) into sensitive cells. For all points after 3 Gy, two groups were observed. Group 1, T98G and T98G-U87; group 2, U87 and T98G-U87 + Lat or Jas 2 h after TNTs, n = 5–6, $p \leq 0.005$. Data were expressed as mean ± SD.

(F) Quantification of survival of sensitive cells to TMZ/IR treatment, U87, in our co-culture system. Separation of both cell types by a semipermeable membrane (8 μm) that enables TNT formation demonstrated that TNTs are essential to transmit the survival factor(s) into susceptible GBM cells (T98G-U87 + TMZ+ 8-μm membrane). Furthermore, the physical movement of the membrane to disrupt TNT formation prevented the adaptation of sensitive GBM cells to TMZ/IR treatment. For all points after 3 Gy, two groups were observed. Group 1, U87; group 2, T98G, T98G-U87, and T98G-U87 + TMZ+8-μm membrane, n = 5–6, $p \leq 0.005$. Data were expressed as mean ± SD.

contacts between resistant and sensitive GBM cells were required for the adaptation to TMZ/IR treatment, we separated both cell types with an 8-μm membrane to enable only TNT formation. We selected a pore size of 8 μm because cell bodies are too big to pass through, but TNTs of different sizes can cross the filter. Cell-to-cell contact was required for the adaptation. However, the use of 0.4-μm filters did not provide treatment adaptation, probably due that TNT formation was compromised. Thus, using the 8-μm barrier, sensitive cells

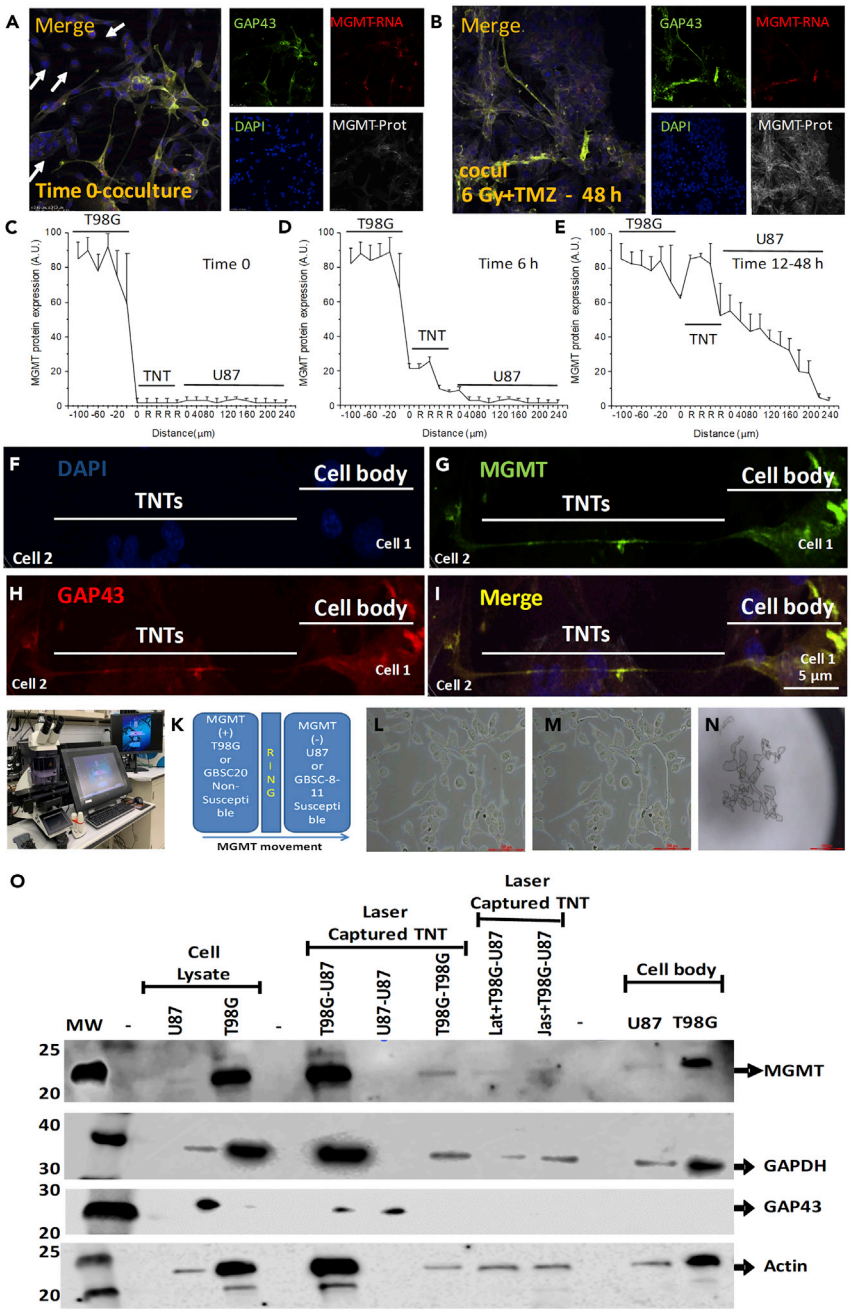

Figure 4. TNTs Enable the Transfer of MGMT Protein, but Not Its mRNA, from Resistant to Sensitive Cells to TMZ/IR Treatment: A Novel Mechanism of Tumor Adaptation to Therapy

(A) Time course of MGMT protein and mRNA spread between resistant and sensitive cells to treatment. Immune staining for GAP43 or protein 14-3-3γ, both TNT markers; DAPI; MGMT protein; and MGMT mRNA analysis by confocal microscopy of our co-culture system. A representative example of staining at the interface before treatment (Time 0, co-culture).

(B) Representative staining after 48 h post-treatment with 6 Gy IR. MGMT protein spread in TNT-dependent manner.

(C) Quantification of positive pixels for MGMT protein in our confocal images using our co-culture system at time 0 before TMZ and IR treatment.

(D) Quantification of MGMT protein up to 6 h post-TNT formation.

(E) Diffusion of MGMT protein into TNTs and U87 cells 12 to 48 h after TMZ and IR treatment. In contrast, MGMT mRNA did not spread into TNTs and U87 cells (see Supplemental Information, Figure S3).

Figure 4. *Continued*

(F–I) Confocal analysis to denote the differences in TNTs and cell bodies as well as MGMT expression partners at the interface between both cell types. The oriented expression, cell localization, and distribution are essential for our next set of experiments involving laser capture microdissection.

(J) The equipment used.

(K) The co-culture model used to separate cell bodies from U87 and T98G cells as well as TNTs.

(L) The bright-field picture of our co-culture system in the laser capture slices.

(M) The cell bodies after TNT laser capture microdissection.

(N) The laser capture micro-dissected material observed by bright field. For TNT analysis, at least 7,000 TNT processes were required.

(O) Western blot analysis of laser micro-dissected material. Cell lysate indicates that only T98G cells are positive for MGMT protein (cell lysate). Laser captured material showed that TNTs between T98G and U87 concentrate MGMT protein when compared with other TNTs isolated from U87-U87 and T98G-T98G co-cultures. Blocking the formation of TNTs after 2 h post-treatment (TMZ, IR, or combination of both treatments) with latrunculin (lat) or jasplakinolide (Jas) prevented MGMT redistribution into the TNTs. The cell body of the cells was similar to the cell lysate experiments after 3–6 h post-treatment. GAPDH, GAP43, and actin were used as loading controls to assure that a significant amount of protein was loaded in each well. In all lines, 100 μg protein was loaded. n = 3 separate experiments.

become resistant to therapy, as demonstrated previously (Figure 3F, pink line, T98G-U87 + TMZ+8-μm membrane). In conclusion, cell-to-cell communication mediated by TNTs between both GBM, one sensitive and another resistant to TMZ/IR treatment, communicates protective factor(s) enabling cells sensitive to TMZ/IR treatment to adapt to and survive it. We believe that our data identify a novel mechanism of tumor adaptation to the current therapies that could provide new avenues to treat GBM.

MGMT (O^6-Alkylguanine DNA Alkyltransferase), Is a Key DNA Repair Enzyme Transferred via TNTs that Protects Susceptible Cells to TMZ/IR Treatment

We hypothesized that the enhanced expression of TNTs induced in GBM cells in response to TMZ/IR treatment enables the lateral transfer of molecule(s)/factors that protect cancer-sensitive cells against the cytotoxic effects of TMZ/IR. As described previously, MGMT was a candidate that promotes TMZ resistance, and we used a candidate approach to examine MGMT in TNTs. To support this notion, a literature review revealed that MGMT mRNA is expressed in T98G cells but not in U87 cells (Lan et al., 2016). Although direct evidence is lacking, MGMT promoter methylation has previously been shown to be predictive of IR response in patients in the absence of TMZ treatment, implying that MGMT may play a broad role in general treatment resistance to cytotoxic therapies (Rivera et al., 2010).

Following this rationale, we first determined the expression and distribution of MGMT mRNA and protein in our co-culture system after TMZ/IR treatment (Figure 4). To identify both cell types, the TNTs between them, and the MGMT (mRNA and protein) distribution, staining for nuclei (DAPI, blue staining), a TNT marker (GAP43 or protein 14-3-3γ, green staining), MGMT mRNA (red staining), and MGMT protein (white staining) was performed. As expected, T98G cells were positive for MGMT mRNA and protein (Figures 4A and 4B). In comparison, U87 were negative or poorly expressing as previously reported (Lan et al., 2016; Minata et al., 2019) (Figures 4A and 4B). GAP43 mainly localized in TNTs and MGMT mRNA in control conditions colocalized with MGMT protein (Figure 4A). However, upon IR or TMZ + IR treatment, TNT numbers increased, GAP43 or 14-3-3γ staining was stronger, and MGMT protein, but not its mRNA, showed overlap with GAP43 or 14-3-3γ along TNTs (Figure 4B). Quantification of the confocal images by determining the number of positive pixels in our co-culture indicated that most MGMT protein was in T98G cells as expected, and there was none in the ring (R) area or in U87 cells in contact with the ring at time 0 (Figure 4C). After 6 h treatment with TMZ, IR, or a combination of both, the amount of MGMT protein moved into the ring where the TNT-like structures were present, as shown in Figures 4B and 4D. In addition, after 6 h TNT contact, it was possible to detect MGMT in TNT structures and positivity in U87 cells (Figure 4D). However, this increase in MGMT protein within TNTs was not associated with increased expression or movement of MGMT mRNA into TNTs or U87 cells (see Figure S3). At later time points, 12–48 h post-treatment there was a further increase in MGMT protein, but not its mRNA (Figure S3), diffusion into TNT structures, and U87 cells (Figure 4E). The MGMT diffusion was induced by TMZ/IR treatment and resulted in the protection of sensitive cells to the therapy, preventing their apoptosis. Furthermore, blocking the formation of TNTs with latrunculin, Lat, or jasplakinolide, jas (10 nM), after 2 h post-TNT formation prevented the diffusion of MGMT protein from resistant cells into susceptible cells, preventing the adaptation of sensitive cells to TMZ/IR treatment (see time course in Figures 4C–4E). Conditioned medium of T98G cells into U87 cells under control and TMZ/IR conditions did not replicate the data, indicating that cell-to-cell communication

and TNT formation is essential for the transfer of MGMT protein and subsequent protection against TMZ/IR treatment.

To demonstrate that MGMT protein can diffuse via TNTs, first we identified TNTs and the cell body as denoted in Figures 3F–3I, using staining for DAPI (nucleus), MGMT protein, GAP43 or 14-3-3γ (a TNT marker), and the merge of these three colors (Figures 4F–4I). Thus, based on the staining profile and localization of the cells and the TNT processes on the plate, we used laser capture micro-dissection to isolate TNTs and the cell bodies of both cell types using the equipment shown in Figure 4J and the co-culture system (Figure 4K). After, laser capture isolation of cell bodies and TNTs, bright-field imaging enabled us to confirm the proper isolation of cell bodies or TNTs (Figures 4L–4N demonstrate the purity of the collected samples, before and after, as well as the collected material for analysis).

To demonstrate that MGMT protein was concentrated in TNTs and diffused into sensitive cells in response to TMZ/IR treatment, we laser capture isolated around 7,000 TNTs with a length of 30–250 μm to obtain enough protein to run western blots to quantify the amount of MGMT protein in the cell bodies as well as within the TNTs. As indicated in Figure 4O, cell lysate from U87 cells was negative for MGMT protein (cell lysate, U87). In contrast, lysate from T98G cells was positive for MGMT protein (cell lysate, T98G).

Laser captured TNT processes isolated from co-cultures of T98G and U87 cells indicated that the MGMT protein was concentrated within the TNT process (laser captured TNT, T98G-U87, 6–18 h post-TNT communication). These data indicate that the MGMT protein moved into the TNT process. In contrast, laser capture of TNTs generated by co-cultures of U87 with U87 cells, as well as T98G with T98G cells subjected to H_2O_2 or TMZ/IR treatment did not induce re-distribution of MGMT protein into the TNTs (Figure 4O, laser captured TNTs, U87-U87 and T98G-T98G, respectively). Thus, there is a gradient of MGMT expression to move the MGMT protein into the TNT. Similar data of GAP43, a TNT marker, was found that mostly accumulated in TNT between U87 and T98G cells (Figure 4O).

Furthermore, blocking TNT formation and associated transport induced by TMZ/IR treatment with the addition of Lat or Jas (added 2 h post-induction of TNT formation, 10 nM) prevented the diffusion or transport of MGMT into the TNT process (Figure 4O, Lat + T98G-U87 or Jas + T98G-U87, laser captured TNTs). Analysis of the cell body of the cells subjected to TNT laser capture indicated that MGMT protein was only present in the T98G cells, but not in the U87 cells, as expected (cell body, 6–12 h post-TNT communication, U87, and T98G, Figure 4O). Our data demonstrate that TNTs between heterogeneous GBM cell populations help tumor cells to survive therapy by spreading MGMT from cells expressing the protein into cells with an insufficient amount of the protective protein against TMZ/IR.

MGMT Protein, but Not Its mRNA, Colocalizes with TNT Markers in Clinical Specimens

To demonstrate that our *in vitro* findings can be observed in clinical specimens, we analyzed human resected GBM and breast cancer (BC) tumors for expression of TNT biomarkers (GAP43 or 14-3-3γ), TNT-like structures, and the colocalization of MGMT protein and mRNA with TNT-like processes.

To perform these experiments, we examined by immunofluorescence staining and subsequent confocal microscopy the expression levels, distribution, and colocalization of these markers *in vivo* (see Table S3 for patient information) (Figure 5). Immunostaining for nuclei (DAPI), 14-3-3γ or GAP43 (a TNT marker), MGMT protein (MGMT Prot), and MGMT-mRNA was performed. GBM tissues showed expression of GAP43 or 14-3-3γ, both TNT markers, to much higher levels, when compared with tissue sections obtained from individuals without GBM or BC or to the adjacent normal tissue (compare Figures 5B and 5D to the controls Figures 5A and 5C, respectively). Normal brain (Figure 5A) or breast (Figure 5C) tissues showed low levels of expression of protein 14-3-3γ and GAP43 (Figures 5A and 5C). In these tissues, MGMT mRNA mostly colocalized with MGMT protein, and the distribution was highly localized into small cell clusters (Figures 5A and 5C). However, in cancer specimens, MGMT mRNA and protein expression increased and became more diffused for MGMT protein, but not for MGMT mRNA (Figures 5B and 5D). Insets in Figures 5A–5D denote the unusual distribution of TNT-like processes (in green) and the clear diffusion of MGMT proteins from cells with MGMT mRNA as well as the localization of MGMT protein with TNT biomarkers (Figure 5). Quantification of the tissue staining using an imaging software, NIS elements, indicated that TNT marker expression increased in all GBM and BC cases (Figure 5E). Examination of the colocalization of TNT markers, GAP-43 and 14-3-3γ, with MGMT protein indicated that at least 60% to 80% of the

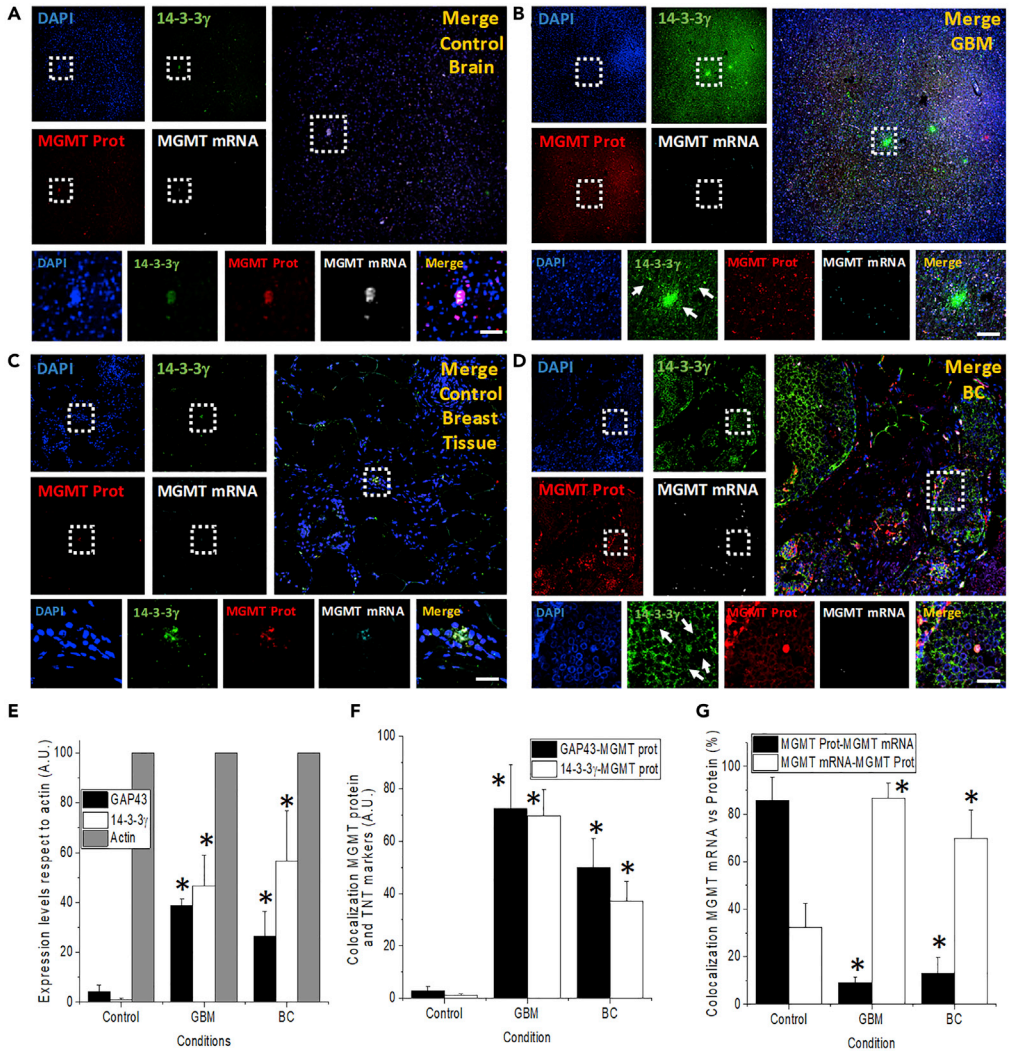

Figure 5. TNT Biomarker Expression Increases in GBM and Breast Cancer

MGMT protein, but not its mRNA, colocalizes with TNT markers. The human brain and breast tissues isolated from patients, healthy and resected tumors, were analyzed by immunostaining for DAPI (nucleus, blue), GAP43 or protein 14-3-3γ (a marker for TNTs, green), MGMT protein (DNA repair enzyme, red), and MGMT mRNA (MGMT RNA scope, white staining, Cy5).

(A) Distribution of the markers in healthy brain tissue. MGMT protein and mRNA, as well as protein 14-3-3γ, were low to undetectable (n = 3–5).

(B) Tissue staining using GBM resected tumors (III and IV degree) indicates that TNT biomarkers, as well as MGMT protein expression, increased. MGMT mRNA remains highly localized as control conditions.

(C and D) Tissue staining of normal and ductal carcinoma with similar results as GBM. Dotted boxes are amplifications of the large pictures for every panel. Arrows represent TNT-like structures in GBM and breast cancer. Scale bar, 20 μm.

(E) The quantification or GAP43 and protein 14-3-3γ in GBM and breast cancer (BC) tissues. Actin (phalloidin staining) was used as a control.

(F) Quantification of the colocalization of TNT markers (GAP43 or 14-3-3γ) with MGMT protein.

(G) Colocalization of MGMT protein with its mRNA and MGMT mRNA with MGMT protein. The reason for performing the reverse colocalization is the low abundance of clusters of MGMT mRNA within the tumor and the extensive spread of MGMT protein in association with TNT markers. *$p \leq 0.002$ when compared with control conditions, n = 6–12, when compared with untreated conditions, data were expressed as mean ± SD.

proteins colocalized with TNT markers in tumor tissue (Figure 5F). Similar data were found for orthotopic xenograft mice models were GBM stem cells are injected into the cortex, and tumor growth was examined (Figure S4). The non-cell injection did not show any non-specific staining for human MGMT-protein, GAP43,

or MGMT mRNA (Figures S4A–S4E). Microinjection of glioma cells negative for MGMT did not show non-specific staining for MGMT protein or mRNA and minimal induction of GAP43 (Figures S4F–S4J). However, microinjection of GBM stem cells and intracranial tumor growth induced infiltration of tumor cells into the mice cortex. MGMT protein diffused long distances in association with GAP43 expression and some MGMT mRNA expression (Figures S4K–S4O), suggesting a similar mechanism of MGMT spread than primary human tumors. Overall, our data suggest that MGMT mRNA is still expressed only in a small population of cells within the tumor, but the MGMT protein diffuses into neighboring areas via TNTs, which contribute to MGMT protein diffusion and spread.

DISCUSSION

GBM is the most aggressive form of brain cancer, and the majority of patients will succumb to the disease within 2 years of diagnosis. Typical characteristics of GBM include intratumoral heterogeneity, lack of T cell infiltration, and extensive vascularization, which have been implicated in resistance to chemo-radiation, inexorable recurrence, and relapse; however, the exact mechanisms are unknown.

In this report, we demonstrate that oxidative stress and TMZ/IR treatment induces the formation of TNTs, enabling the transport of key protective factors against tumor treatment between interconnected cancer cells. TNT generation and communication were mostly unidirectional from the cells resistant to therapy into sensitive cells leading to the rescue of the sensitive cells from apoptosis induced by TMZ/IR treatment. We identified that MGMT protein, but not its mRNA, is one of the molecules transported via TNTs. However, we cannot discard that other molecules or organelles are transmitted by TNTs. Currently, the interaction between TMZ/IR remains unclear; however, TNT formation protects cells from DNA-associated damage, and we propose that TNTs mediate the adaptation of the tumor to treatment by mediating a metabolic/DNA repair cooperation among different cells within the tumor.

TNTs are thin and long cellular processes that communicate between two or more cells, resulting in a bridge that allows direct communication between the cytoplasm of the connected cells. We have already characterized at least two different kinds of TNTs, a fused process with the target cell and a second one that is a synaptic type with several proteins at the tip, including connexin43. The first one enables the transfer of small molecules as well as large organelles, including mitochondria and lysosomes. The second type probably has a cutoff of exchange of around 1.2 kDa (Gerdes et al., 2007). However, each TNT is composed of several tangled processes with different permeabilities. The identification of TNT processes *in vivo* during the pathogenesis of HIV, BC, and GBM opens a novel layer to the complexity of the development and adaptation of the tumor.

Here, we speculate that TNT communication enables the transfer of additional DNA repair enzymes that help the survival of sensitive cells to TMZ/IR treatment. We have now identified that TNTs are an effective "highway" to spread TMZ/IR resistance. Thus, beyond conventional dogma, wherein MGMT promoter methylation and silencing is an established model of TMZ sensitization in GBM, our study has uncovered a novel mechanism by which TMZ resistance can be spread via TNT-mediated transfer of MGMT. Concerning the major implication of our findings is the fast and effective transfer of MGMT protein from MGMT mRNA-positive cells into neighboring cells with minimal MGMT expression via TNT. Our results indicate that cytotoxic treatments increase the adaption of the tumor cells to overcome cell death. These can have significant clinical implications, and TNTs can become an important therapeutic target to reduce or prevent MGMT spread into tumor areas that are sensitive to treatment.

Interestingly, the mechanism of therapy adaptation was unrelated to the status of MGMT mRNA translation or MGMT methylation of the promoter (Chen et al., 2018a; Jiang et al., 2018; Rivera et al., 2010; Xi et al., 2018), because no changes in mRNA MGMT expression were detected. Our data contribute to the poor knowledge of the mechanisms of tumor survival and adaptation to TMZ/IR treatment. Furthermore, our data contribute to answering the critical question of whether MGMT is inducible during tumorigenesis, or it is induced following treatment with TMZ/IR. Indeed, given that several studies indicate that MGMT activity level increased during therapy (Christmann et al., 2011; Kitange et al., 2009; Wiewrodt et al., 2008), there are significant inconsistencies about MGMT gene levels and MGMT activity that cannot be explained only by promotor methylation or protein activity. In agreement, all the MGMT detection methods, including promoter methylation-specific PCR, immunohistochemistry, MGMT protein, and mRNA expression, cannot explain all the resistance and adaptation to treatment data available (Brell et al., 2011; Maxwell

et al., 2006). Interestingly, our data indicate that the process of protection and MGMT diffusion is highly regulated due to several reasons: first, in our model, a TNT-directed communication for at least 6 h is required to protect sensitive cells to treatment from TMZ + IR toxicity; thus, a constant flux of MGMT protein is necessary as well as increased synthesis of the protein to protect both cells, resistant and sensitive; a second option is that TNT formation and the diffusion of MGMT could actvate additional mechanisms of TMZ+IR protection in the sensitive targeted cells to further extend the TNT mediated protective effects. Furthermore, our data only demonstrated that MGMT is transmitted by a TNT-mediated mechanism; however, several organelles and other proteins are transmitted with unknown metabolic, gene editing, epigenetic, and inflammatory conditions to adapt the healthy and tumor cells to perpetuate the survival of the tumor even in adverse conditions. We believe that MGMT is only one of the metabolic modifiers "shared" by TNTs with neighboring cells, but other cargo, as well as different cell targets such as immune cells and fibroblasts, may have a different cargo and adaptation. In this article, we propose that one of these mechanisms related to tumor heterogeneity is related to TNT formation and transport of MGMT protein into areas of the tumor with excellent response to treatment. Overall, TNT formation and transport enable the diffusion of MGMT protein "priming" susceptible areas of the tumor to become unresponsive to current therapies.

In conclusion, our data identified a novel mechanism of cell-to-cell communication between tumor cells. TNTs are critical for tumor cells to adapt and survive treatment, by the exchange of several cytoplasmic modifiers, including the enzyme MGMT. As a concerning note, IR and, to a lesser extent, TMZ treatment accelerates TNT formation, MGMT protein diffusion, and adaptation to treatment. We propose that TNTs are essential for tumor development, adaptation to treatment, and recurrence by creating a cooperative network within the tumor and surrounding cells to survive and are attractive targets for therapeutic intervention in GBM and other cancers.

Limitations of the Study

Although TNTs corresponds to a recently discovered cell-to-cell communication system the mechanisms of TNT formation, cargo, and biological effects in the targeted cells are still poorly understood. The identification of MGMT as a TNT cargo between GBM cells does not discard the possibility that other enzymes or organelles also are transferred between connected cells. A potential concern that was not addressed in our current report is the increased TNT formation and MGMT spread upon TMZ + radiation, suggesting that treatment alone can prime the tumor to become adapted and resistant to therapy. This point was not examined in the current publication and warrants further investigation. Cell lines, T98G and U87 cells, may be not represented by the phenotype of primary GBM stem cells in the tumor. Currently, we and others are examining these concerns by isolating and repeating the presented experiments in primary GBM cells.

Resource Availability

Lead Contact

Further information and requests for resources and reagents should be directed to, and will be fulfilled by, the Lead Contact, Eliseo Eugenin (eleugeni@utmb.edu).

Materials Availability

This study did not generate new unique reagents. Further information and requests for reagents should be directed to and will be fulfilled by the Lead Contact, Dr. Eliseo Eugenin (eleugeni@UTMB.edu). Sharing reagents with academic or company researchers may require M.T.A. agreements.

Data and Code Availability

This study did not generate/analyze datasets/code.

METHODS

All methods can be found in the accompanying Transparent Methods supplemental file.

SUPPLEMENTAL INFORMATION

Supplemental Information can be found online at https://doi.org/10.1016/j.isci.2020.101450.

ACKNOWLEDGMENTS

We thank the NNTC and Neurobiobank for providing tissues. This work was funded by The National Institute of Mental Health grant, MH096625, the National Institute of Neurological Disorders and Stroke, NS105584, and UTMB internal funding (to E.A.E).

AUTHOR CONTRIBUTIONS

Conceptualization and methodology, S.V., A.A., K.P.L.B., G.O., and E.A.E. Investigation, S.V., A.A., K.P.L.B., and E.A.E. Resources, S.V., K.P.L.B., and E.A.E. Writing, S.V, K.P.L.B., G.O., and E.A.E. Supervision, K.P.L.B. and E.A.E.

DECLARATION OF INTERESTS

The authors declare no competing interest.

Received: March 16, 2020
Revised: April 28, 2020
Accepted: August 10, 2020
Published: September 25, 2020

REFERENCES

Abe, H., Natsumeda, M., Kanemaru, Y., Watanabe, J., Tsukamoto, Y., Okada, M., Yoshimura, J., Oishi, M., and Fujii, Y. (2018). MGMT expression contributes to temozolomide resistance in H3K27M-mutant diffuse midline gliomas and MGMT silencing to temozolomide sensitivity in IDH-mutant gliomas. Neurol. Med. Chir (Tokyo) *58*, 290–295.

Abounit, S., Bousset, L., Loria, F., Zhu, S., de Chaumont, F., Pieri, L., Olivo-Marin, J.C., Melki, R., and Zurzolo, C. (2016a). Tunneling nanotubes spread fibrillar alpha-synuclein by intercellular trafficking of lysosomes. EMBO J. *35*, 2120–2138.

Abounit, S., Delage, E., and Zurzolo, C. (2015). Identification and characterization of tunneling nanotubes for intercellular trafficking. Curr. Protoc. Cell Biol. *67*, 12 10 11–12. 10 21.

Abounit, S., Wu, J.W., Duff, K., Victoria, G.S., and Zurzolo, C. (2016b). Tunneling nanotubes: a possible highway in the spreading of tau and other prion-like proteins in neurodegenerative diseases. Prion *10*, 344–351.

Abounit, S., and Zurzolo, C. (2012). Wiring through tunneling nanotubes–from electrical signals to organelle transfer. J. Cell Sci. *125*, 1089–1098.

Ady, J., Thayanithy, V., Mojica, K., Wong, P., Carson, J., Rao, P., Fong, Y., and Lou, E. (2016). Tunneling nanotubes: an alternate route for propagation of the bystander effect following oncolytic viral infection. Mol. Ther. Oncol. *3*, 16029.

Arevalo, A.S.T., Erices, J.I., Uribe, D.A., Howden, J., Niechi, I., Munoz, S., Martin, R.S., and Monras, C.A.Q. (2017). Current therapeutic alternatives and new perspectives in glioblastoma multiforme. Curr. Med. Chem. *24*, 2781–2795.

Ariazi, J., Benowitz, A., De Biasi, V., Den Boer, M.L., Cherqui, S., Cui, H., Douillet, N., Eugenin, E.A., Favre, D., Goodman, S., et al. (2017a). Tunneling nanotubes and gap junctions-their role in long-range intercellular communication during development, health, and disease conditions. Front. Mol. Neurosci. *10*, 333.

Ariazi, J., Benowitz, A., De Biasi, V., Den Boer, M.L., Cherqui, S., Cui, H., Douillet, N., Eugenin, E.A., Favre, D., Goodman, S., et al. (2017b). Tunneling nanotubes and gap junctions-their role in long-range intercellular communication during development, health, and disease conditions. Front. Mol. Neurosci. *10*, 333.

Arora, A., and Somasundaram, K. (2019). Glioblastoma vs temozolomide: can the red queen race be won? Cancer Biol. Ther. *20*, 1083–1090.

Astanina, K., Koch, M., Jungst, C., Zumbusch, A., and Kiemer, A.K. (2015). Lipid droplets as a novel cargo of tunnelling nanotubes in endothelial cells. Sci. Rep. *5*, 11453.

Austefjord, M.W., Gerdes, H.H., and Wang, X. (2014). Tunneling nanotubes: Diversity in morphology and structure. Commun. Integr. Biol. *7*, e27934.

Bahadur, S., Sahu, A.K., Baghel, P., and Saha, S. (2019). Current promising treatment strategy for glioblastoma multiform: a review. Oncol. Rev. *13*, 417.

Batash, R., Asna, N., Schaffer, P., Francis, N., and Schaffer, M. (2017). Glioblastoma multiforme, diagnosis and treatment; recent literature review. Curr. Med. Chem. *24*, 3002–3009.

Brell, M., Ibanez, J., and Tortosa, A. (2011). O6-Methylguanine-DNA methyltransferase protein expression by immunohistochemistry in brain and non-brain systemic tumours: systematic review and meta-analysis of correlation with methylation-specific polymerase chain reaction. BMC Cancer *11*, 35.

Chen, L., Wang, Y., Liu, F., Xu, L., Peng, F., Zhao, N., Fu, B., Zhu, Z., Shi, Y., Liu, J., et al. (2018a). A systematic review and meta-analysis: association between MGMT hypermethylation and the clinicopathological characteristics of non-small-cell lung carcinoma. Sci. Rep. *8*, 1439.

Chen, X., Zhang, M., Gan, H., Wang, H., Lee, J.H., Fang, D., Kitange, G.J., He, L., Hu, Z., Parney, I.F., et al. (2018b). A novel enhancer regulates MGMT expression and promotes temozolomide resistance in glioblastoma. Nat. Commun. *9*, 2949.

Christmann, M., Verbeek, B., Roos, W.P., and Kaina, B. (2011). O(6)-Methylguanine-DNA methyltransferase (MGMT) in normal tissues and tumors: enzyme activity, promoter methylation and immunohistochemistry. Biochim. Biophys. Acta *1816*, 179–190.

Delgado-Lopez, P.D., and Corrales-Garcia, E.M. (2016). Survival in glioblastoma: a review on the impact of treatment modalities. Clin. Transl. Oncol. *18*, 1062–1071.

Desir, S., Dickson, E.L., Vogel, R.I., Thayanithy, V., Wong, P., Teoh, D., Geller, M.A., Steer, C.J., Subramanian, S., and Lou, E. (2016). Tunneling nanotube formation is stimulated by hypoxia in ovarian cancer cells. Oncotarget *7*, 43150–43161.

Ding, Z., Issekutz, T.B., Downey, G.P., and Waddell, T.K. (2003). L-selectin stimulation enhances functional expression of surface CXCR4 in lymphocytes: implications for cellular activation during adhesion and migration. Blood *101*, 4245–4252.

Eugenin, E.A., Branes, M.C., Berman, J.W., and Saez, J.C. (2003). TNF-alpha plus IFN-gamma induce connexin43 expression and formation of gap junctions between human monocytes/macrophages that enhance physiological responses. J. Immunol. *170*, 1320–1328.

Eugenin, E.A., Eckardt, D., Theis, M., Willecke, K., Bennett, M.V., and Saez, J.C. (2001). Microglia at brain stab wounds express connexin 43 and in vitro form functional gap junctions after treatment with interferon-gamma and tumor necrosis factor-alpha. Proc. Natl. Acad. Sci. U S A *98*, 4190–4195.

Eugenin, E.A., Gaskill, P.J., and Berman, J.W. (2009a). Tunneling nanotubes (TNT) are induced by HIV-infection of macrophages: a potential

mechanism for intercellular HIV trafficking. Cell Immunol. *254*, 142–148.

Eugenin, E.A., Gaskill, P.J., and Berman, J.W. (2009b). Tunneling nanotubes (TNT): a potential mechanism for intercellular HIV trafficking. Commun. Integr. Biol. *2*, 243–244.

Gerdes, H.H., Bukoreshtliev, N.V., and Barroso, J.F. (2007). Tunneling nanotubes: a new route for the exchange of components between animal cells. FEBS Lett. *581*, 2194–2201.

Gerdes, H.H., and Carvalho, R.N. (2008). Intercellular transfer mediated by tunneling nanotubes. Curr. Opin. Cell Biol. *20*, 470–475.

Gerdes, H.H., Rustom, A., and Wang, X. (2013). Tunneling nanotubes, an emerging intercellular communication route in development. Mech. Dev. *130*, 381–387.

Gousset, K., Schiff, E., Langevin, C., Marijanovic, Z., Caputo, A., Browman, D.T., Chenouard, N., de Chaumont, F., Martino, A., Enninga, J., et al. (2009). Prions hijack tunnelling nanotubes for intercellular spread. Nat. Cell Biol. *11*, 328–336.

Hegi, M.E., Diserens, A.C., Gorlia, T., Hamou, M.F., de Tribolet, N., Weller, M., Kros, J.M., Hainfellner, J.A., Mason, W., Mariani, L., et al. (2005). MGMT gene silencing and benefit from temozolomide in glioblastoma. N. Engl. J. Med. *352*, 997–1003.

Hegi, M.E., Genbrugge, E., Gorlia, T., Stupp, R., Gilbert, M.R., Chinot, O.L., Nabors, L.B., Jones, G., Van Criekinge, W., Straub, J., et al. (2019). MGMT promoter methylation cutoff with safety margin for selecting glioblastoma patients into trials omitting temozolomide: a pooled analysis of four clinical trials. Clin. Cancer Res. *25*, 1809–1816.

Hegi, M.E., and Stupp, R. (2015). Withholding temozolomide in glioblastoma patients with unmethylated MGMT promoter–still a dilemma? Neuro Oncol. *17*, 1425–1427.

Jackson, C.B., Noorbakhsh, S.I., Sundaram, R.K., Kalathil, A.N., Ganesa, S., Jia, L., Breslin, H., Burgenske, D.M., Gilad, O., Sarkaria, J.N., et al. (2019). Temozolomide sensitizes MGMT-deficient tumor cells to ATR inhibitors. Cancer Res. *79*, 4331–4338.

Jiang, S., Rui, Q., Wang, Y., Heo, H.Y., Zou, T., Yu, H., Zhang, Y., Wang, X., Du, Y., Wen, X., et al. (2018). Discriminating MGMT promoter methylation status in patients with glioblastoma employing amide proton transfer-weighted MRI metrics. Eur. Radiol. *28*, 2115–2123.

Jung, E., Osswald, M., Blaes, J., Wiestler, B., Sahm, F., Schmenger, T., Solecki, G., Deumelandt, K., Kurz, F.T., Xie, R., et al. (2017). Tweety-homolog 1 drives brain colonization of gliomas. J. Neurosci. *37*, 6837–6850.

Kim, G.W., Lee, D.H., Yeon, S.K., Jeon, Y.H., Yoo, J., Lee, S.W., and Kwon, S.H. (2019). Temozolomide-resistant glioblastoma depends on HDAC6 activity through regulation of DNA mismatch repair. Anticancer Res. *39*, 6731–6741.

Kitange, G.J., Carlson, B.L., Schroeder, M.A., Grogan, P.T., Lamont, J.D., Decker, P.A., Wu, W., James, C.D., and Sarkaria, J.N. (2009). Induction of MGMT expression is associated with temozolomide resistance in glioblastoma xenografts. Neuro Oncol. *11*, 281–291.

Kuang, Y.Q., Pang, W., Zheng, Y.T., and Dupre, D.J. (2012). NHERF1 regulates gp120-induced internalization and signaling by CCR5, and HIV-1 production. Eur. J. Immunol. *42*, 299–310.

Lan, F., Yang, Y., Han, J., Wu, Q., Yu, H., and Yue, X. (2016). Sulforaphane reverses chemo-resistance to temozolomide in glioblastoma cells by NF-kappaB-dependent pathway downregulating MGMT expression. Int. J. Oncol. *48*, 559–568.

Lee, S.Y. (2016). Temozolomide resistance in glioblastoma multiforme. Genes Dis. *3*, 198–210.

Mansouri, A., Hachem, L.D., Mansouri, S., Nassiri, F., Laperriere, N.J., Xia, D., Lindeman, N.I., Wen, P.Y., Chakravarti, A., Mehta, M.P., et al. (2019). MGMT promoter methylation status testing to guide therapy for glioblastoma: refining the approach based on emerging evidence and current challenges. Neuro Oncol. *21*, 167–178.

Maxwell, J.A., Johnson, S.P., Quinn, J.A., McLendon, R.E., Ali-Osman, F., Friedman, A.H., Herndon, J.E., 2nd, Bierau, K., Bigley, J., Bigner, D.D., et al. (2006). Quantitative analysis of O6-alkylguanine-DNA alkyltransferase in malignant glioma. Mol. Cancer Ther. *5*, 2531–2539.

Melamed, J.R., Morgan, J.T., Ioele, S.A., Gleghorn, J.P., Sims-Mourtada, J., and Day, E.S. (2018). Investigating the role of Hedgehog/GLI1 signaling in glioblastoma cell response to temozolomide. Oncotarget *9*, 27000–27015.

Minata, M., Audia, A., Shi, J., Lu, S., Bernstock, J., Pavlyukov, M.S., Das, A., Kim, S.H., Shin, Y.J., Lee, Y., et al. (2019). Phenotypic plasticity of invasive edge glioma stem-like cells in response to ionizing radiation. Cell Rep. *26*, 1893–1905.e7.

Nam, J.Y., and de Groot, J.F. (2017). Treatment of glioblastoma. J. Oncol. Pract. *13*, 629–638.

Okafo, G., Prevedel, L., and Eugenin, E. (2017). Tunneling nanotubes (TNT) mediate long-range gap junctional communication: implications for HIV cell to cell spread. Sci. Rep. *7*, 16660.

Osswald, M., Jung, E., Sahm, F., Solecki, G., Venkataramani, V., Blaes, J., Weil, S., Horstmann, H., Wiestler, B., Syed, M., et al. (2015). Brain tumour cells interconnect to a functional and resistant network. Nature *528*, 93–98.

Pegg, A.E. (2000). Repair of O(6)-alkylguanine by alkyltransferases. Mutat. Res. *462*, 83–100.

Polak, R., de Rooij, B., Pieters, R., and den Boer, M.L. (2015). B-cell precursor acute lymphoblastic leukemia cells use tunneling nanotubes to orchestrate their microenvironment. Blood *126*, 2404–2414.

Preusser, M., Charles Janzer, R., Felsberg, J., Reifenberger, G., Hamou, M.F., Diserens, A.C., Stupp, R., Gorlia, T., Marosi, C., Heinzl, H., et al. (2008). Anti-O6-methylguanine-methyltransferase (MGMT) immunohistochemistry in glioblastoma multiforme: observer variability and lack of association with patient survival impede its use as clinical biomarker. Brain Pathol. *18*, 520–532.

Raghavan, S., Baskin, D.S., and Sharpe, M.A. (2020). A "Clickable" probe for active MGMT in glioblastoma demonstrates two discrete populations of MGMT. Cancers (Basel) *12*, 453.

Rahman, M.A., Gras Navarro, A., Brekke, J., Engelsen, A., Bindesboll, C., Sarowar, S., Bahador, M., Bifulco, E., Goplen, D., Waha, A., et al. (2019). Bortezomib administered prior to temozolomide depletes MGMT, chemosensitizes glioblastoma with unmethylated MGMT promoter and prolongs animal survival. Br. J. Cancer *121*, 545–555.

Rivera, A.L., Pelloski, C.E., Gilbert, M.R., Colman, H., De La Cruz, C., Sulman, E.P., Bekele, B.N., and Aldape, K.D. (2010). MGMT promoter methylation is predictive of response to radiotherapy and prognostic in the absence of adjuvant alkylating chemotherapy for glioblastoma. Neuro Oncol. *12*, 116–121.

Roehlecke, C., and Schmidt, M.H.H. (2020). Tunneling nanotubes and tumor microtubes in cancer. Cancers *12*, 857.

Silber, J.R., Bobola, M.S., Blank, A., and Chamberlain, M.C. (2012). O(6)-methylguanine-DNA methyltransferase in glioma therapy: promise and problems. Biochim. Biophys. Acta *1826*, 71–82.

Souriant, S., Balboa, L., Dupont, M., Pingris, K., Kviatcovsky, D., Cougoule, C., Lastrucci, C., Bah, A., Gasser, R., Poincloux, R., et al. (2019). Tuberculosis exacerbates HIV-1 infection through IL-10/STAT3-dependent tunneling nanotube formation in macrophages. Cell Rep. *26*, 3586–3599.e7.

St-Coeur, P.D., Cormier, M., LeBlanc, V.C., Morin, P.J., and Touaibia, M. (2016). Effect of O6-substituted guanine analogs on O6-methylguanine DNA-methyltransferase expression and glioblastoma cells viability. Med. Chem. *13*, 28–39.

Tardivel, M., Begard, S., Bousset, L., Dujardin, S., Coens, A., Melki, R., Buee, L., and Colin, M. (2016). Tunneling nanotube (TNT)-mediated neuron-to neuron transfer of pathological Tau protein assemblies. Acta Neuropathol. Commun. *4*, 117.

Thomas, A., Tanaka, M., Trepel, J., Reinhold, W.C., Rajapakse, V.N., and Pommier, Y. (2017). Temozolomide in the era of precision medicine. Cancer Res. *77*, 823–826.

Towner, R.A., Smith, N., Saunders, D., Brown, C.A., Cai, X., Ziegler, J., Mallory, S., Dozmorov, M.G., Coutinho De Souza, P., Wiley, G., et al. (2019). OKN-007 increases temozolomide (TMZ) sensitivity and suppresses TMZ-resistant glioblastoma (GBM) tumor growth. Transl. Oncol. *12*, 320–335.

Tsai, C.K., Huang, L.C., Wu, Y.P., Kan, I.Y., and Hueng, D.Y. (2019). SNAP reverses temozolomide resistance in human glioblastoma multiforme cells through down-regulation of MGMT. FASEB J. *33*, 14171–14184.

Valdebenito, S., Lou, E., Baldoni, J., Okafo, G., and Eugenin, E. (2018). The novel roles of connexin channels and tunneling nanotubes in cancer pathogenesis. Int. J. Mol. Sci. *19*, 1270.

Wang, X., and Gerdes, H.H. (2012). Long-distance electrical coupling via tunneling nanotubes. Biochim. Biophys. Acta *1818*, 2082–2086.

Wang, Y., Cui, J., Sun, X., and Zhang, Y. (2011). Tunneling-nanotube development in astrocytes depends on p53 activation. Cell Death Differ. *18*, 732–742.

Weil, S., Osswald, M., Solecki, G., Grosch, J., Jung, E., Lemke, D., Ratliff, M., Hanggi, D., Wick, W., and Winkler, F. (2017). Tumor microtubes convey resistance to surgical lesions and chemotherapy in gliomas. Neuro Oncol. *19*, 1316–1326.

Weller, M., Stupp, R., Reifenberger, G., Brandes, A.A., van den Bent, M.J., Wick, W., and Hegi, M.E. (2010). MGMT promoter methylation in malignant gliomas: ready for personalized medicine? Nat. Rev. Neurol. *6*, 39–51.

Wick, W., and Platten, M. (2018). Understanding and treating glioblastoma. Neurol. Clin. *36*, 485–499.

Wiewrodt, D., Nagel, G., Dreimuller, N., Hundsberger, T., Perneczky, A., and Kaina, B. (2008). MGMT in primary and recurrent human glioblastomas after radiation and chemotherapy and comparison with p53 status and clinical outcome. Int. J. Cancer *122*, 1391–1399.

Xi, Y.B., Guo, F., Xu, Z.L., Li, C., Wei, W., Tian, P., Liu, T.T., Liu, L., Chen, G., Ye, J., et al. (2018). Radiomics signature: a potential biomarker for the prediction of MGMT promoter methylation in glioblastoma. J. Magn. Reson. Imag. *47*, 1380–1387.

Yi, G.Z., Huang, G., Guo, M., Zhang, X., Wang, H., Deng, S., Li, Y., Xiang, W., Chen, Z., Pan, J., et al. (2019). Acquired temozolomide resistance in MGMT-deficient glioblastoma cells is associated with regulation of DNA repair by DHC2. Brain *142*, 2352–2366.

Zhang, J., Stevens, M.F., and Bradshaw, T.D. (2012a). Temozolomide: mechanisms of action, repair and resistance. Curr. Mol. Pharmacol. *5*, 102–114.

Zhang, J., Stevens, M.F., and Bradshaw, T.D. (2012b). Temozolomide: mechanisms of action, repair and resistance. Curr. Mol. Pharmacol. *5*, 102–114.

Zhang, L., and Zhang, Y. (2015). Tunneling nanotubes between rat primary astrocytes and C6 glioma cells alter proliferation potential of glioma cells. Neurosci. Bull. *31*, 371–378.

Zhu, D., Tan, K.S., Zhang, X., Sun, A.Y., Sun, G.Y., and Lee, J.C. (2005). Hydrogen peroxide alters membrane and cytoskeleton properties and increases intercellular connections in astrocytes. J. Cell Sci. *118*, 3695–3703.

iScience, Volume *23*

Supplemental Information

Tunneling Nanotubes Mediate Adaptation of Glioblastoma Cells to Temozolomide and Ionizing Radiation Treatment

Silvana Valdebenito, Alessandra Audia, Krishna P.L. Bhat, George Okafo, and Eliseo A. Eugenin

Supplemental Information

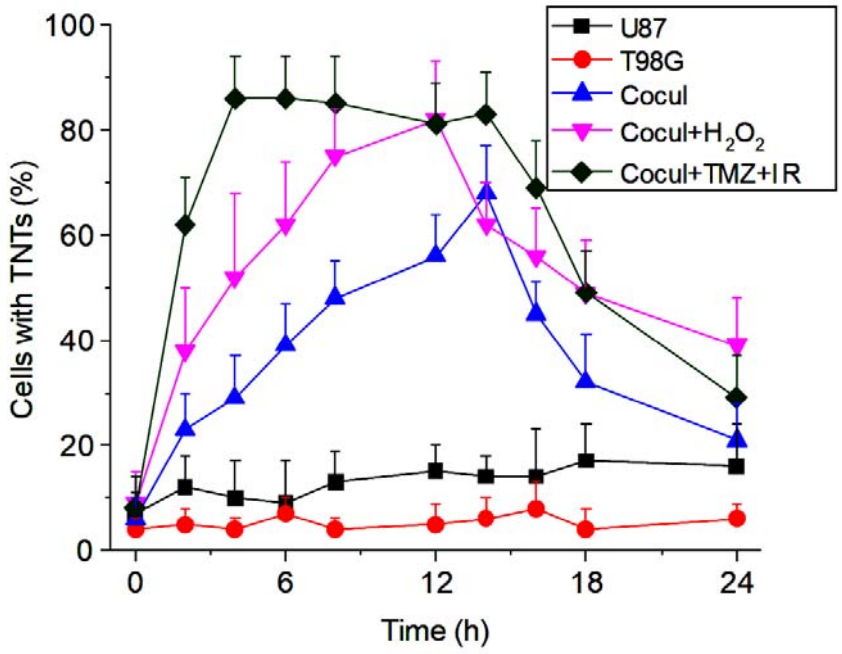

Figure S1 (Related to Figure 1). TNTs are induced in our co-culture system upon oxidative stress or TMZ/IR treatment. Quantification of TNTs in our co-culture system in response to H_2O_2, IR, and TMZ. All data were expressed as mean±S.D.

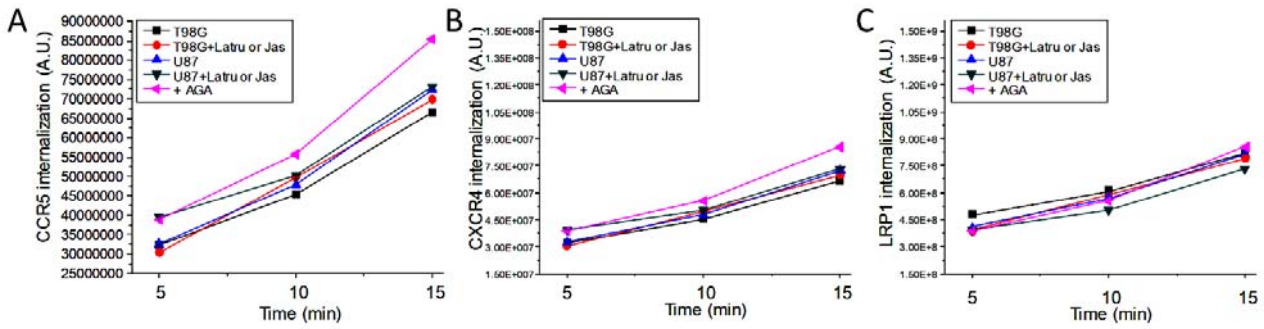

Figure S2 (Related to Figure 1 and 2). Internalization experiments using biotinylated antibodies for CCR5 (A), CXCR4 (B), and LRP1 (C) in the function of time in the presence and absence of mild actin or gap junction blockers that reduce the formation of TNTs and/or associated transport. No differences in receptor internalization were observed with any of the treatments used to block TNTs. The main reason to observe a strong effect of these blockers on TNT formation and transport is the high amount of actin polymerization required for TNT formation, associated transport, and collapse of the process. This highly dependent mechanism on actin only has been described at this magnitude in cell division and TNT formation. Thus, our blockers at the concentration used do not affect the trafficking of high recycling receptor types on the plasma membrane that relay on active actin signaling and a significant rate of polymerization and de-polymerization. n=4, data were expressed as mean±S.D.

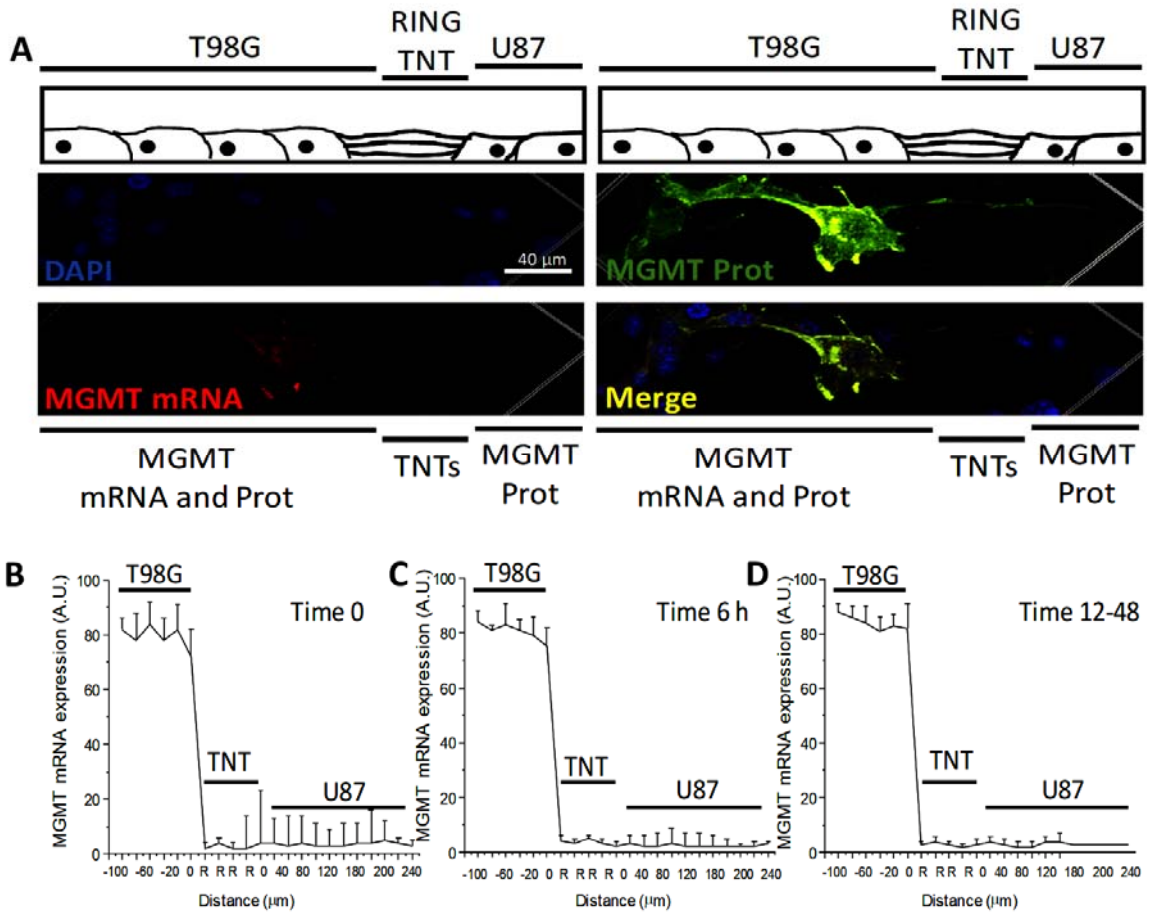

Figure S3 (Related to Figure 4). MGMT mRNA is not transported via TNTs. The time course of MGMT mRNA spread between resistant and sensitive cells to treatment. Immune staining for GAP43 or protein 14-3-3γ, both TNT markers, DAPI, MGMT protein, and MGMT mRNA analysis by confocal microscopy of our co-culture system. (A) The cartoon represents our co-culture system and corresponding confocal images for DAPI, MGMT protein, mRNA, and the merge of all colors at the interface after TMZ and IR treatment. (B) Quantification of positive pixels for MGMT mRNA in our confocal images using our co-culture system at time 0 before TMZ and IR treatment. (C) Quantification of MGMT mRNA up to 6 h post-TNT formation. (D) Corresponds to the diffusion of MGMT mRNA into TNTs and U87 cells after 12 to 48 h post-TMZ/IR treatment. n=4-5.

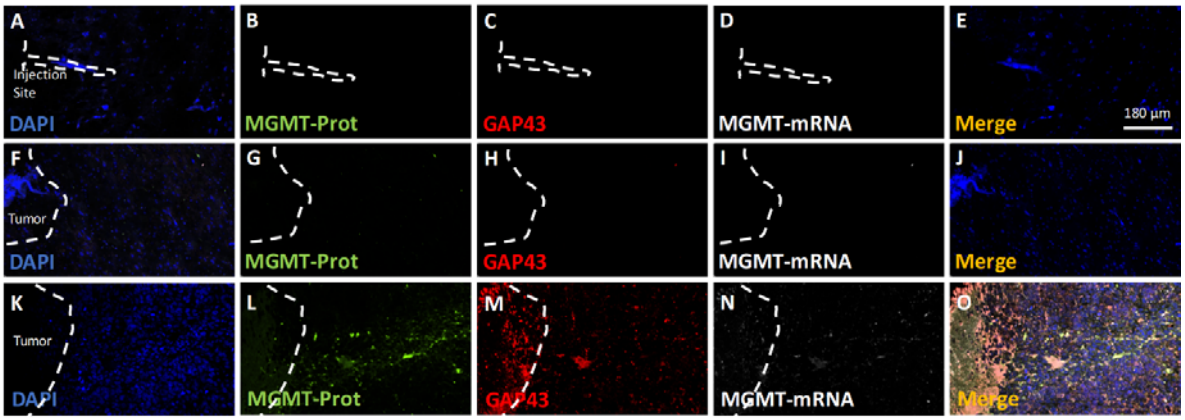

Figure S4 (Related to Figure 5): Glioblastoma stem-like cells were isolated from patients undergoing surgery at M.D. Anderson Medical Center and injected into the cortex of mice to generate an orthotopic xenograft animal. Tissue sections were stained for nuclei (DAPI, blue staining), MGMT protein (MGMT-Prot, green staining), GAP43 (red), and MGMT mRNA (white staining) as well as the merge of all colors. (A-E) Mice cortex with no injected cells to demonstrate the specificity of the staining and tumor growth. (F-G) Injection of glioblastoma cells (negative for MGMT) into the cortex with non-unspecific staining. (K-O) Microinjection of glioblastoma stem-like cells into the cortex and diffusion of MGMT protein into the mice cortex from the primary tumor in association with GAP43 expression. Segmented lines denote the border of the tumor or injection site (n=3-5).

Tables

Table S1 (Related to Figure 1 and 2): TNT Characteristic in Cell Lines

Condition	TNT stability (min)	TNT Length (µm)	TNT vesicular transport (% of TNTs)	TNT Branching (% of TNTs)
U87-Control	1.65±0.98 (T) 2.31±0.25 (S)	8.55±3.69 (Sh) 38.25±11.6 (Lo)	0.12±0.05	0±0
U87-H_2O_2	3.65±2.67 (T) 18.65±10.1 (S)	19.3±11.0 (Sh) 99.4±21.2 (Lo)	5.04±2.39	1.02±0.23
U87-IR	28.05±21.23(T) 161.01±87.1(S)	17.04±11 (Sh) 256.99±101 (Lo)	10.02±3.66	11.45±3.33
U87-TMZ	5.66±2.36(T) 31.09±11.1(S)	20.05±8.8 (Sh) 45.85±10.1 (Lo)	0.58±0.08	1.57±0.89
U87-IR+TMZ	26.81±10.8(T) 125.6±29.9(S)	23.3±9.08 (Sh) 111±20.6 (Lo)	15.78±7.88±	16.87±8.47
T98G-Control	1.09±1.05(T) 2.08±0.85(S)	6.78±2.89 (Sh) 22.28±6.79 (Lo)	0.17±0.11	0±0
T98G-H_2O_2	2.87±0.98(T) 15.58±5.08 (S)	23.09±10.1 (Sh) 112.85±20.9(Lo)	8.09±3.69	3.68±1.08
T98G-IR	35.85±10.58(T) 159.87±20.1(S)	28.8±7.09 (Sh) 269.78±36.9(Lo)	16.98±9.78	21.05±8.09
T98G-TMZ	6.71±2.01(T) 29.89±8.87(S)	26.78±10.5 (Sh) 39.87±8.88 (Lo)	1.68±0.98	2.68±1.05
T98G- IR+TMZ	35.91±8.67(T) 89.78±10.7(S)	28.98±4.58 (Sh) 165.5±29.8 (Lo)	19.87±6.78	19.7±5.68
Co-Control	2.09±1.08(T) 4.52±2.78(S)	12.69±4.51 (Sh) 35.65±8.24 (Lo)	3.05±11.85	0±0
Co-H_2O_2	6.72±2.78(T) 25.98±7.05 (S)	41.1±8.98 (Sh) 168.5±30.2 (Lo)	9.78±4.05	2.22±1.05
Co-IR	49.98±7.09(T) 198.7±29.8(S)	45.71±12.3 (Sh) 284.6±29.7 (Lo)	29.58±9.87	30.89±10.08
Co-TMZ	39.78±9.78(T) 177.8±40.9(S)	39.9±4.01 (Sh) 120.0±36.5 (Lo)	3.5±1.98	2.08±0.68
Co-IR+TMZ	46.98±10.8(T) 200.98±19.8(S)	59.8±6.54 (Sh) 298.85±84.2(Lo)	39.87±5.05	30.36±9.99

Notes: (T) Transient, (S) stable, (Sh) Short, (Lo) Long

Data were expressed as mean±S.D., n=12-15. Data were pooled during the time course examined (0 to 48 h post-treatment).

Table S2 (Related to Figure 2): Characteristic of the cell types used

Cell type	TMZ sensitive	Radiation Sensitive	MGMT expression
U87 cells	10 μM	Yes	Low
T98G	≥500 μM	No	High

Table S3: Patient information (brain and breast cancer, related to Figure 5)

Patient-condition	Age	Sex	IDH status	Cancer-grade
Healthy				
Healthy 1	42	M	Unknown	N/A
Healthy 2	49	M	Unknown	N/A
Healthy 3	59	M	Unknown	N/A
Healthy 4	55	F	Unknown	N/A
Brain Tumors				
Oligodendroglioma	42	M	Unknown	2
Astrocytoma	46	M	R132H	2
Astrocytoma	35	F	Unknown	3
Astrocytoma	61	M	Unknown	3
Glioblastoma	55	F	Unknown	4
Oligoastrocytoma	36	M	Unknown	2
Breast Cancer				
Invasive Ductal Carcinoma	51	F	Unknown	2
Invasive Ductal Carcinoma	42	F	Unknown	3
Invasive Ductal Carcinoma	33	F	Unknown	2
Invasive Ductal Carcinoma	38	F	Unknown	2
Invasive Ductal Carcinoma	47	F	Unknown	3

Transparent Methods

Materials: DMEM, fetal bovine serum (FBS), penicillin/streptomycin (P/S), and trypsin-EDTA were from Thermo-Fisher (Grand Island, NY). Purified mouse IgG_{2B} and IgG_1 myeloma proteins were from Cappel Pharmaceuticals, Inc. DAPI, anti-rabbit, and anti-mouse conjugated to Alexa were from Thermo-Fisher (Eugene, OR). The *in situ* cell death detection kit (TUNEL) was from Roche (Mannheim, Germany).

Glioblastoma Cell Lines: Cell lines, U87, and T98G were purchased from the ATCC (Manassas, VA). U87 and T98G were grown in DMEM medium supplemented with 2-10% FBS and pen/strep and maintained at 37°C in a humidified incubator supplied with 5% CO_2. Mycoplasma test was performed every 4 months, as well as new cell batches, which were ordered from the ATCC for scientific rigor.

Cell culture and IR. To perform these experiments, we used the Stem cell Isolation and Xenotransplantation Core Facility at the Albert Einstein College of Medicine (Bronx, NY). The equipment used was a Shepherd Mark I Irradiator Model 68 filed with 4000-6000 of Cesium (Ci) 137. Single-dose exposure ranged from 0 to 12 Gy. After IR, the medium was changed, and fresh medium was added. The cells were incubated for 2 or 7 days to detect clonal expansion and degree of apoptosis, as previously described (Chalmers et al., 2009). Using these cells, a co-culture model was set between T98G cells at the center of the plate, while U87 sensitive cells to treatment were at the periphery of the plate. The main reasons to perform this co-culture were to maximize the numbers of TNTs per area (interface), a localized formation (easier isolation), and directed communication.

Clinical Tissue sample collection. Human brain tissues were obtained from M.D. Anderson Medical Center. Normally, we obtained resected brain tissues with the core tumor and the edge as well as some small sections of “healthy” tissue. All our studies were approved by the M.D. Anderson and UTMB institutional review board. Tissues were obtained from astro- and oligodendroglioma stages III and IV (see Table 3). Tissues were immediately transferred to Biological safety Class II cabinet and dissected into different regions and fixed in 10 % neutral buffered formalin for at least 24 h, dehydrated, and paraffin-embedded. Serial sections from each block were prepared for Hematoxylin and Eosin staining, and the stained slides were imaged at 20X using an image capture device (Hamamatsu, Japan), and images were reviewed by an experienced pathologist.

qRT-PCR. Total RNA was extracted from GBM cells using TRIzol and the phase-lock system (Eppendorf, Hauppauge, NY, USA), following the manufacturer’s instructions. cDNA synthesis was performed using 2 µg total RNA using the iScript cDNA synthesis kit (Bio-Rad, Hercules, CA, USA) according to the manufacturer’s instructions. The amplified cDNA was used to amplify and quantify MGMT and GAPDH mRNA expression by qPCR using Absolute Blue qPCR SYBR low ROX mix in a StepOnePlus thermocycler (Applied Biosystems, Life Technologies, Carlsbad, CA, USA). The primers used correspond to GAPDH forward: 5′-GAGAAGTATGACAACAGCCTCAA-3′, GAPDH reverse: 5′AGTCCTTCCACGATACCAAAG-3′; MGMT forward: 5′- GTGATTTCTTACCAGCAATTAGCA -3′, MGMT reverse: 5′-CTGCTGCAGACCACTCTGTG -3′. The program used was denaturation for 15 min at 95°C and 40 cycles of denaturation, 15 s at 95°C; anneal, 30 s at 60°C; and amplification, 30 s at 72°C. Expression was determined using the ΔΔCT method, according to the CT values.

Live Cell Imaging. For analysis two different cell culture systems were used — first, single-cell cultures in regular tissue culture plates. Confluence used was 50 to 70 % to enable TNT extension and communication and reduce the possibility of overgrowth that can compromise TNT identification and characterization. Our imaging system corresponds to an Axio-observed Z1 with 3 redundant incubation systems with CO_2 and humidity control to avoid any significant variations in temperature, CO_2, or humidity. We imaged for 24 to 48 h, recording every 30 seconds to 1 min.

Image analysis. Raw data for TNTs and other membrane protrusions were obtained using the Zen software (Zeiss Software, Germany). As described in the result section, several rules were considered to identify a TNT. The more important was cell to cell distance and cell to cell communication by live-cell imaging. Filopodium did not comply with these rules. For confocal analysis, 3D deconvolutions were obtained using NIS elements (Nikon, Japan). Quantification of colocalization, intensities, and lengths, as well as stability, was performed in NIS elements and Image J using the criteria described in the result section.

Laser capture microdissection. Pure cultures or co-cultures of cells were grown on director slices (Expression Pathology, Culver City, CA) for laser capture. To preserve TNTs structure and communication, we fix the cells in 1.5 % PFA, and then we increased the concentration to 3.0 % after 20 min, later we added 100% ethanol to dry the slides and proceed to cut the TNTs. Most isolation was performed under control

conditions or co-cultures to reach 7,000 TNTs isolated per condition for qRT-PCR and Western blot for the MGMT protein. To perform the isolations, we used LMD6000 equipment with the respective software (Leica, Germany). For Western blot and mRNA, the polled samples were dissolved in RIPA lysis buffer, and then RNA was isolated using the RNeasy Micro Kit (Qiagen, #74004, Valencia, CA). RNA content was determined using a Nanodrop 2000 spectrophotometer (Thermo Scientific, Wilmington, DE).

Western Blot Analysis. Cells or laser captured material were lysed with RIPA buffer (Cell Signaling, Beverly, MA) containing protease and phosphate inhibitors (Cell Signaling, Danvers, MA), and 100 µg (or total collected material in the case of laser capture microdissection) of protein were electrophoresed on a 4-20% polyacrylamide gel (Bio-Rad, CA), and transferred to nitrocellulose membranes. Membranes were probed with rabbit monoclonal antibodies to MGMT (Thermofisher, Carlsbad, CA), actin (Santa Cruz Biotechnology, Dallas, TX), and GAPDH (Cell Signaling, Danvers, MA). Densitometric analysis was performed using NIH ImageJ software.

Immunofluorescence. Human GBM cells were grown on glass coverslips, fixed and permeabilized in 70% ethanol for 20 min at -20^{o}C. Cells were incubated in blocking solution for 30 min at room temperature and then in primary antibody (anti-GAP43, anti-14-3-3γ, and anti-MGMT, or isotype controls: both 1:50) overnight at 4^{o}C. Cells were washed several times with PBS at room temperature and incubated with phalloidin conjugated to Texas Red to identify actin filaments and/or the appropriate secondary antibody conjugated to FITC (Sigma, St. Louis, MO) for 1 h at room temperature,

followed by another wash in PBS for 1 h. Cells were then mounted using antifade reagent with DAPI, and cells were examined by confocal microscopy using an A1 Nikon confocal microscope with spectral detection (Tokyo, Japan). To ensure proper staining, several negative and positive controls were used as well as matching antibody isotypes, as we described (Prevedel et al., 2019). Some of the controls included MGMT negative and positive tumors, pre-absorption with the recombinant protein, and isolation for laser capture and proteomics. In all our experiments, no unspecific staining was observed.

Electron microscopy. Cells were fixed for 30 min at RT using 4% paraformaldehyde, 2% glutaraldehyde, buffered with 0.1 M sodium cacodylate. Cells were dried with hexamethyldisilazane until fully dry under a fume hood. The cells were analyzed using a Zeiss SUPRA 40 field emission scanning electron microscopy (SEM) and placed on a fitted mold for the holder. The holder was calibrated, and cells were imaged at various magnifications, as indicated, with an accelerating voltage of 3 kV. This protocol allows us to maintain TNT structure and cell shape (see details in the result section).

RNA scope for MGMT mRNA. RNAscope (RNAscope® Fluorescent Multiplexed reagent kit, Advanced Cell Diagnostics) was used as per the manufacturer's protocol and adjusted for dual detection of MGMT protein and TNT markers by immunofluorescence, as we recently described for HIV conditions (Castellano et al., 2019; Ganor et al., 2019; Prevedel et al., 2019).

Orthotopic Xenograft Animal Models. Glioblastoma stem-like cells were isolated from patients undergoing surgery at M.D. Anderson Medical Center. 500K cells were injected into the

cortex and sacrificed upon showing signs of brain disease as indicated (Moreno et al., 2017). Mice that presented neurological symptoms (i.e., seizures, inactivity, or ataxia) or that were moribund were sacrificed, and brains were fixed in formalin and stained with H&E to confirm the presence of a tumor. All animal procedures were reviewed and approved by the Institutional Animal Care and Use Committee at M.D. Anderson, Texas.

Statistical analysis. Information on the statistical tests used, and the exact values of n (number of experiments) can be found in Figure Legends. All statistical analyses were performed using GraphPad Prism 6.0 (GraphPad Software Inc.). The statistical tests were chosen according to the following: two-tailed paired or unpaired t-test was applied on datasets with a normal distribution (Kolmogorov-Smirnov test), whereas two-tailed Mann-Whitney (unpaired test) or Wilcoxon matched-paired signed-rank tests were used otherwise. $p < 0.05$ was considered as the level of statistical significance.

REFERENCES

Castellano, P., Prevedel, L., Valdebenito, S., and Eugenin, E.A. (2019). HIV infection and latency induce a unique metabolic signature in human macrophages. Sci Rep *9*, 3941.
Chalmers, A.J., Ruff, E.M., Martindale, C., Lovegrove, N., and Short, S.C. (2009). Cytotoxic effects of temozolomide and radiation are additive- and schedule-dependent. Int J Radiat Oncol Biol Phys *75*, 1511-1519.
Ganor, Y., Real, F., Sennepin, A., Dutertre, C.A., Prevedel, L., Xu, L., Tudor, D., Charmeteau, B., Couedel-Courteille, A., Marion, S.*, et al.* (2019). HIV-1 reservoirs in urethral macrophages of patients under suppressive antiretroviral therapy. Nat Microbiol *4*, 633-644.
Moreno, M., Pedrosa, L., Pare, L., Pineda, E., Bejarano, L., Martinez, J., Balasubramaniyan, V., Ezhilarasan, R., Kallarackal, N., Kim, S.H.*, et al.* (2017). GPR56/ADGRG1 Inhibits Mesenchymal Differentiation and Radioresistance in Glioblastoma. Cell reports *21*, 2183-2197.
Prevedel, L., Ruel, N., Castellano, P., Smith, C., Malik, S., Villeux, C., Bomsel, M., Morgello, S., and Eugenin, E.A. (2019). Identification, Localization, and Quantification of HIV Reservoirs Using Microscopy. Curr Protoc Cell Biol *82*, e64.

Reagents

Reagent or Resource	Source	Identifier
Antibodies		
Anti-Human GAP43 /EP890Y	Abcam	Cat# ab75810; https://www.abcam.com/gap43-antibody-ep890y-ab75810.html#top-600
Anti-Human 14-3-3 gamma/YWHAG	Abcam	Cat# ab155050; https://www.abcam.com/14-3-3-gammaywhag-antibody-ab155050.html
GAPDH (14C10) anti-Human	Cell Signaling	Cat# 2118L; https://media.cellsignal.com/pdf/2118.pdf
MGMT Anti-Human (MT23.3)	Invitrogen/Thermo Fisher Scientific	Cat# RL242361; RRID: AB_2533219
Actin (C-2) Anti-Human	Santa Cruz Biotechnology	Cat# SC-8432; https://datasheets.scbt.com/sc-8432.pdf
Anti-Human Connexin 43	Sigma Aldrich	Cat# C6219; https://www.sigmaaldrich.com/content/dam/sigma-aldrich/docs/Sigma/Datasheet/3/c6219dat.pdf
Normal Anti-Mouse Igg	Santa Cruz Biotechnology	Cat# SC-2025; https://datasheets.scbt.com/sc-2025.pdf
Normal Anti-Rabbit Igg	Sigma Aldrich	Cat# A-9919; https://www.sigmaaldrich.com/content/dam/sigma-aldrich/docs/Sigma/Datasheet/6/a9919dat.pdf
Donkey Anti-Rabbit, Alexa Fluor 488	Invitrogen/Thermo Fisher Scientific	Cat# A21206; RRID: AB_2535792
Goat Anti-Mouse, Alexa Fluor 568	Invitrogen/Thermo Fisher Scientific	Cat# A11031; RRID: AB_144696
Chemicals, Peptides, and Recombinant Proteins		
Human MGMT protein	Abcam	Cat# ab79251
Critical Commercial Assays		
RNAScope Probe-Hs-MGMT	ACDbio	Cat# 588941
DAPI	Thermo Fisher Scientific	Cat# P36931
SuperSignal WestPico Chemiluminescent	Thermo Fisher Scientific	Cat# 34080
Biological Samples		
Patients GB	MD Anderson	N/A

Tissue Samples	Medical School, Houston, Texas	
Cell Lines		
U87 MG	ATCC	Cat# HTB-14
T98G	ATCC	Cat# CLR-1690
Software		
ImageJ	ImageJ	https://imagej.nih.gov/ij/
OriginLab 2019	Origin	https://www.originlab.com/
NIS-elements 2.3	Nikon	https://www.microscope.healthcare.nikon.com/products/software
ZEN 4.7	Zeiss	https://www.zeiss.com/microscopy/us/products/microscope-software/zen.html